Univerzita Karlova v Praze
Matematicko-fyzikální fakulta

Diplomová práce

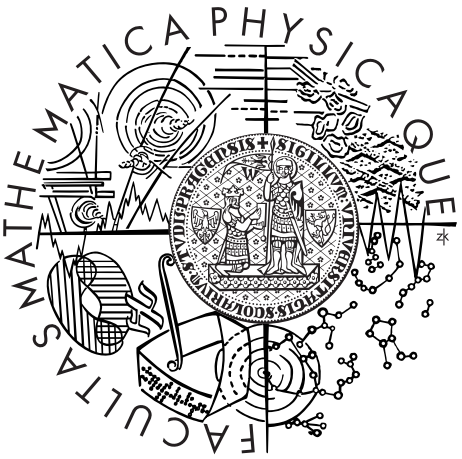

Bc. Martin Hrubovský

Studium termoresponzivních porfyrínů a jejich supramolekulárních komplexů

Katedra makromolekulární fyziky

Vedoucí diplomové práce: RNDr. Hana Kouřilová, Ph.D.

Studijní program: Fyzika

Studijní obor: Fyzika kondenzovaných soustav a materiálů

Praha 2016

Charles University in Prague
Faculty of Mathematics and Physics

MASTER THESIS

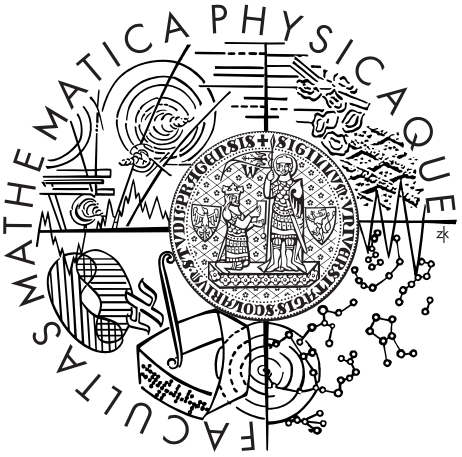

Bc. Martin Hrubovský

Study of thermoresponsive porphyrins and their supramolecular complexes

Department of Macromolecular Physics

Supervisor of the master thesis:	RNDr. Hana Kouřilová, Ph.D.
Study programme:	Physics
Specialization:	Physics of Condensed Matter and Materials

Prague 2016

I am most grateful to my:

- supervisor Hana Kouřilová for her friendly and appreciative leadership, with whom working is a fruitful pastime.
- collaborant Jan Labuta for professional insights, Japanese-like working zeal, providing us with the samples and for spearheading our research
- my consultant and chief of the Department of Macromolecular Physics Lenka Hanyková for always having a tranquil, constructive and apolitical attitude and for giving me the working opportunities to become familiar with the NMR method during my bachelor's studies
- parents Štefan and Alena Hrubovský for giving me care, respect and freedom to become my best self

These people are mentioned separately because I also consider them role models for my development. There are other people directly helpful in creation of this thesis, mostly High Resolution NMR lab colleagues who helped me with technical difficulties or offered their experience, namely Václav Římal, Petr Křišťan and Karel Bernášek and the chemist Jonathan P. Hill who discovered the compounds we study.

I declare that I carried out this master thesis independently, and only with the cited sources, literature and other professional sources.

I understand that my work relates to the rights and obligations under the Act No. 121/2000 Coll., the Copyright Act, as amended, in particular the fact that the Charles University in Prague has the right to conclude a license agreement on the use of this work as a school work pursuant to Section 60 paragraph 1 of the Copyright Act.

In ..... date ..... signature of the author

Název práce: Studium teplotně citlivých porfyrinů a jejich supramolekulárních komplexů

Autor: Bc. Martin Hrubovský

Katedra: Katedra makromolekulární fyziky

Vedoucí diplomové práce: RNDr. Hana Kouřilová, Ph.D., Katedra makromolekulární fyziky

Abstrakt: Venovali sme sa štúdiu látky mezo-tetrakis{3,4,5-tris[2-(2-(2-metoxyetoxy)etoxy)etoxy]fenyl}porfyrín umelo pripravenej v NIMS v Japonsku. Využívali sme NMR spektroskopiu vysokého rozlišenia. Pozorovali sme jej fázovú separáciu LCST-typu (dolná kritická teplota roztoku) a aplikovali sme Floryho-Hugginsovu teóriu polymérnych roztokov aby sme skonštruovali jej fázový diagram (binodálu a spinodálu, krivky fázovej separácie), a tiež sme vyhodnotili jej molárne entropie, entaplie a kritickú teplotu fázovej separácie; aplikáciou Floryho-Hugginsovej teórie sme zistili, že molekuly skúmanej látky tvoria vo vode diméry. Tiež sme sledovali interakcie tejto látky s kyselinou *S*-gáfor-sulfonovou; dozvedeli sme sa, že študovaný porfyrín viaže katióny z roztoku a porfyrínové diméry sa rozpadajú ak je v roztoku dostatok dostupných katiónov pre vznik komplexov. V chloroforme nebola pozorovaná žiadna fázová separácia. Porfyrín netvorí viac než diméry.

Klíčová slova: porfyrin, spektroskopie nukleární magnetické rezonance (NMR), komplex hostitel-host, supramolekulární systémy

Title: Study of thermoresponsive porphyrins and their supramolecular complexes

Author: Bc. Martin Hrubovský

Department: Department of Macromolecular Physics

Supervisor: RNDr. Hana Kouřilová, Ph.D., Department of Macromolecular Physics

Abstract:
We studied the water-soluble artificial compound meso-tetrakis{3,4,5-tris[2-(2-(2-methoxyethoxy)ethoxy)ethoxy]phenyl}porphyrin prepared at NIMS, Japan, using the high-resolution NMR spectroscopy experimental method. We observed its LCST-type phase separation and applied the Flory-Huggins theory of polymer solutions in order to find its phase diagram (binodal and spinodal curves of the phase separation) and we also obtained molar enthalpies, entropies and critical temperatures of its phase separation; from the Flory-Huggins theory we discovered that its molecules form dimers in aqueous solutions. We also studied its host-guest interactions with the *S*-camphorsulfonic acid; we learned that the porphyrin binds cations and the porphyrin dimers break down when dissolved cations are available for complexation. We observed no phase separation in chloroform. We obtained no proof of the existence of molecular stacks larger than dimers.

Keywords: porphyrin, nuclear magnetic resonance (NMR) spectroscopy, host-guest complexes, supramolecular complexes

Contents

Preface

Porphyrins attract attention of researchers because of their ability to form complexes with positively charged molecules, molecules forming hydrogen bonds, molecules with conjugated electron systems and because they can be used to detect enantiopurity of these ligands. When a planar porphyrin forms a complex, it adopts a saddle-like conformation. If the ligand is chiral, a higher degree of asymmetry in porphyrin's conformation is induced and some peaks in NMR spectra undergo splitting linearily dependent on the enantiomeric excess of the ligand. The tetrapyrrolic conjugated electron system in the saddle-like conformation also has different energy levels which changes the porphyrin's color radically.

We study a new group of porphyrins prepared by our colleagues from National Institute for Materials Science in Tsukuba, Japan (NIMS). These exhibit behavior similar to amphiphilic polymers – namely water solubility, temperature-induced phase separation (with LCST for aqueous solutions, UCST for dimethyl sulfoxide) and cononsolvency.

The properties enumerated above could make these porphyrins useful in biophysics, medicine and nanotechnology. While they have properties typical for polymers, the molecules are well-defined and have molecular mass in the order of kilodaltons.

In this thesis, we use the experimental method of nuclear magnetic resonance spectroscopy (NMR) to quantify the phase separation, investigate the porphyrin molecules' interaction with each other and examine the effects of acidity on all of the phenomena. Several micrographs taken using an optical microscope (OM) are also included.

1. Introduction

1.1 Porphyrins

Porphine is a tetrapyrrolic macrocycle, with conjugated π-electron rings, schematically shown in the Figure 1.1. The conjugated π-electron system gives porphine some important properties. Porphine:

- absorbs photons in the visible spectrum
- has propensity for various inter-molecular interactions; namely enabling stacking due to quadrupole and dispersive interactions, and ion binding – strong complexation abilities [1]

Both of the properties above can be fine-tuned by:

- chemical modification of porphine – these modifications are called *porphyrins*
- changing the solvent – effects called *solvatochromism* for optical properties, *hydrophobic interactions* and *cononsolvency* for inter-molecular interactions.

The properties and effects enumerated above are used by living organisms for the purpose of binding other molecules, as is the case for *heme* binding oxygen in human red blood cells or *cobalamin* (vitamin B_{12}) which acts as an enzyme – catalyst for biochemical reactions; or for the energy capture from light, which is the purpose of *chlorophyll* which makes most of the terrestrial flora green. Earth's biosphere as we know it is predicated upon these *porphyrins'* functions. This is summarized in the Table 1.1

Furthermore, research in recent years has shown that achiral porphyrins can be used for chirality detection[2], [3]. When a chiral ligand binds to an achiral porphyrin host, it induces assymetry in the porphyrin's average conformation. This leads to some nuclear sites becoming magnetically inequivalent, which can then be observed as peak splitting linearly dependent on the enantiomeric excess using the Nuclear Magnetic Resonance spectroscopy (NMR, our primary experimental method, see the Section 2.1). However, the splitting gives no information about *which* enantiomer is dominant and the magnitude of the splitting has to be *calibrated case-by-case*. For an example, see the Figure 1.2 with a section of a ^{1}H NMR spectrum of the molecule **DiBrBzOxP** ("**dibr**om**b**en**z**ylated **ox**o**p**orphyrin") studied in [4].

Table 1.1: Examples of important porpyrins

Name	Location	Function	Metal ion
Heme[5]	red blood cells	oxygen transport	Fe^{2+}
Chlorophyll[6]	plants	photosynthesis	Mg^{2+}
Cobalamin (Vit B_{12})[7]	animals, gut bacteria	enzyme	Co^{+}
Corphin[8]	Methanogens	CH_4 production	Ni^{+}
Phthalocyanine[9]	dye industry	monastric blue	-/Cu^{2+}

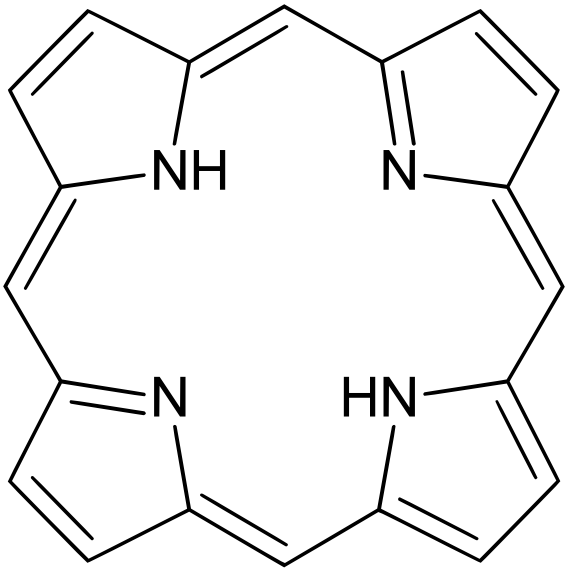

Figure 1.1: The stucture of porphine, molecule with supramolecular behavior and visible spectrum absorption. It can bind metal ions, free H^+, molecules with conjugated electron systems (including itself). Chemical modification and solvent properties can affect the conjugated electron system and its supramolecular interactions. Living organisms use a myriad of porphin derivatives (examples in the Table 1.1 and the Figure 1.3) for several purposes, e.g. binding oxygen, methanogenesis, light energy absorption. A porphin molecule without a guest can be called a *free base*.

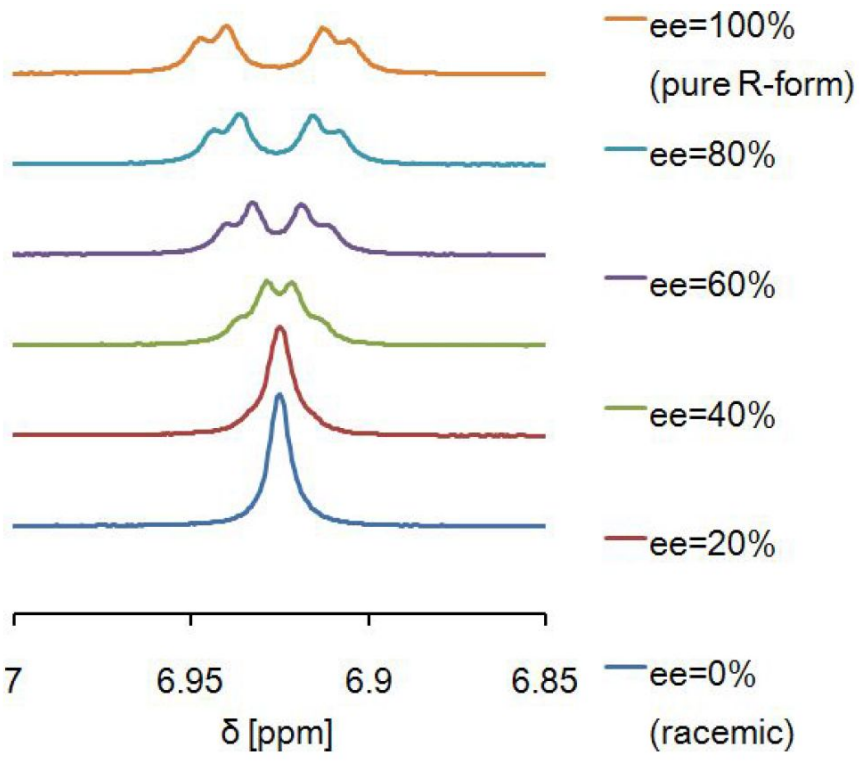

Figure 1.2: Without a ligand, symmetric porphyrins are planar (bottom spectral line). A chiral ligand induces asymmetry in porphyrins' average conformation and this leads to the splitting of peaks which are no longer equivalent. This effect is linearily dependent on the enantiomeric excess of the chiral ligand[4].

Heme B

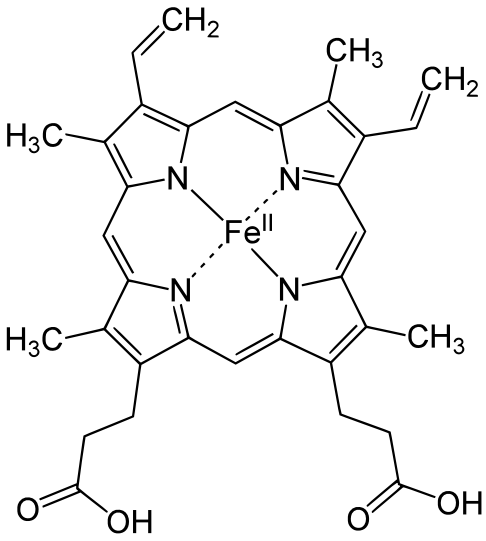

Chlorophyll a

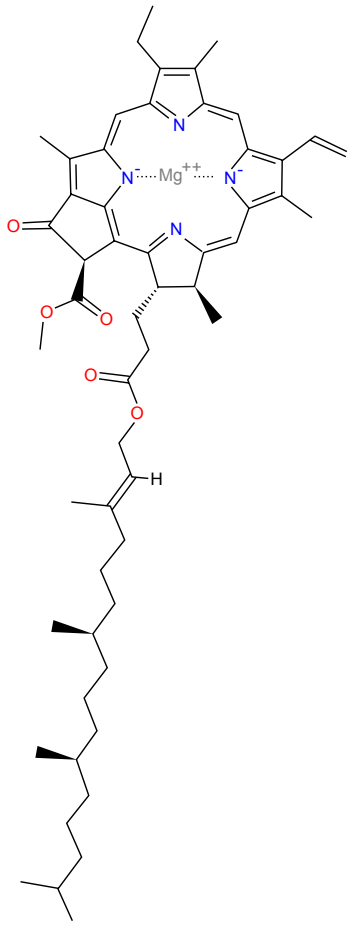

Vitamin B_{12} (cobalamin)

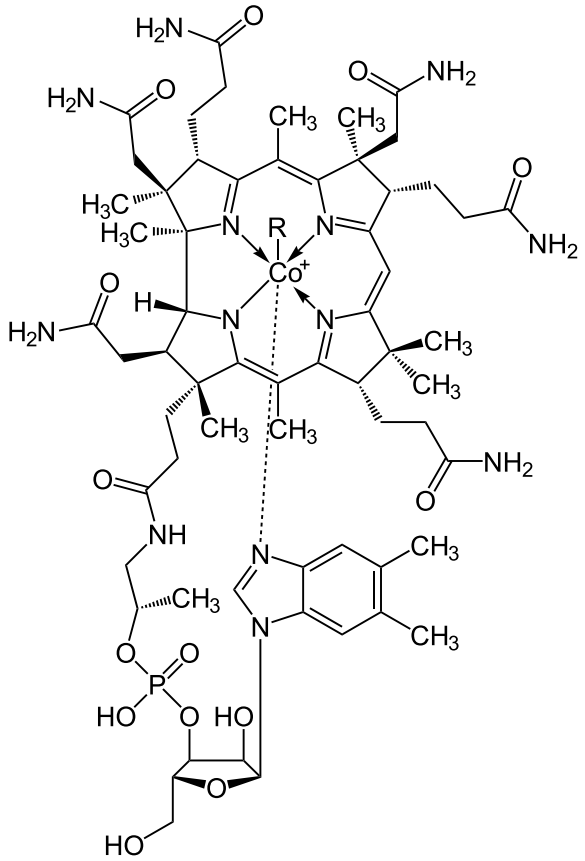

Figure 1.3: Examples of important porphyrins found in nature. *Heme B* is a component of hemoglobin that binds and transports O_2 in our bodies. *Chlorophyll a* is the most common pigment of the photosynthetic pigment group "chlorophyll" that makes most of terrestrial flora green [10]. Vitamin B_{12} is required for normal brain function and metabolism in every cell of our bodies.

1.2 State of the art of supramolecular chemistry

Supramolecular chemistry is the study of *intermolecular interactions* in general. It categorizes the types of interactions, interprets the interactions using thermodynamics and according to the introduction of extensive review of supramolecular chemistry's progress up to 2009 [11], the subject of non-covalent bonding is likely become *the* topic of this century's chemistry. Much of the information below is also from [11].

The purpose of this section is to give a *brief* overview of the currently known inter-molecular interaction *types*, and describe them at least *qualitatively* – how to understand them and whether they are relevant to the object of our study. These inter-molecular interactions are important to review because they are *precisely the properties that we investigate* in this thesis; we need to verify and quantify some of them for the compound **3,4,5-TEG-TPP** described in the Subsection 1.3.

Types of inter-molecular interactions:

- hydrogen bonding
  - relevant:
    - hydrogens from water interact with O in TEG side groups and N on the tetrapyrrolic macrocycle. This increases solubility of **3,4,5-TEG-TPP**.
    - bound protons can form hydrogen bonds with chiral ligands and thus induce asymmetry in the porphyrin, making it sensitive to enantiopurity
- chelation
  - metal ion being bound to several sites in a given molecule
  - not relevant now, because we use pure D_2O and add no metal ions. However, this is a further research suggestion. Natural porphyrins bind ions and become functional pigments.
- ion-π electron interactions
  - conjugated π electrons rings over and under a cyclic molecule are a local increase in electron density and a quadrupole
  - relevant: protons dissociated from acids should bind to the π rings of the porphyrin macrocycle
- electrostatic interaction of approximately point charges
  - relevant: H^+ dissociated from acids should also be attracted to the N atoms of the porphyrin macrocycle
- salt bridges
  - ion pairs bound to one molecule can favorably interact with ion pairs on a different molecule
  - not relevant: **3,4,5-TEG-TPP** contains no ionic bonds; the acid – *S*-camphorsulfonic acid (*S*-CSA) – and the products of its dissociation contain them neither
- dispersive interactions
  - fluctuating electron density can lead to effectively attractive multipole interaction
  - very relevant: the conjugated electrons are a delocalized electron density that is susceptible to external stimuli, and have non-zero quadrupole moment even if left alone. Porphyrins are known to bind aromatic compounds; with ΔG proportional to the number of π-electrons [12]. This effect is sometimes misleadingly called "π-π stacking" [13]
- solvophobic interactions
  - hydrophobic effect – dissolution of a non-polar molecule incurs an entropy penalty due to the reduced number of possible arrangements of surrounding water molecules

  - probably not relevant: although non-polar regions are present, hydrophobic effects are negligible for "complexations with flat surfaces such as porphyrins" [14].

- container-like molecular structure
  - when cavities in molecules are unfavorable for solvent, solute is attracted to the free openings
  - not relevant: **3,4,5-TEG-TPP** has no such cavities

The π-electrons give porphine strong complexation properties. Through π-electron interactions porphine can bind metal ions, acid residues and other molecules with conjugated electron systems including itself. These interactions occur in the gaseous phase and in solvents, where molecules are free to move around. The solubility of porphyrins in both water and organic solvents is typically low, due to the low polarity of their bonds [15].

1.3 3,4,5-TEG-TPP

The object of our study is a porphyrin with full systematic name *meso-tetrakis{3,4,5-tris[2-(2-(2-methoxyethoxy)ethoxy)ethoxy]phenyl}porphyrin*. From now on, we are going to call it **3,4,5-TEG-TPP** (semi-systematic abbreviation of "**t**etra**p**henylated **p**orphyrin with **t**eta**e**thylene **g**lycol-like chains at phenyl sites **3**, **4** and **5**").

This compound was prepared by our colleagues at International Center for Materials Nanoarchitectonics of National Institute for Materials Science (MANA, NIMS) in Tsukuba, prefecture Ibaraki, Japan.

We have already explained what porphyrins are in the Subsection 1.1 and the properties to be observed in the Subsection 1.2. Now we need to specify how the compound **3,4,5-TEG-TPP** differs from other porphyrins in structure and chemical composition and what novel phenomena can be expected as a result.

The most notable properties of **3,4,5-TEG-TPP** and their possible consequences to be verified by our experiments are:

- it is the compound with the *highest symmetry* of all porphyrins from the set of prepared phenylated porphyrins with oligoethylene glycol-like chains.
  - it should not adopt saddle-like conformations or have several atropoisomers
  - this is the reason why we chose to study this molecule in detail first, before the others. It is the simplest one, and could serve as a key for understanding the porphyrins with reduced symmetry.

- on each of the phenyl groups, there are three aliphatic tetra-ethylene glycol-like chains
  - polyethylene glycol being a notoriously hydrophilic polymer should *increase the water solubility* of **3,4,5-TEG-TPP**
  - polyethylene glycol in aqueous solution can undergo phase separation with *lower critical solution temperature* (LCST) at around 85°C [16]
  - these could work as *steric barriers*, restricting surrounding macromolecules from adopting close and parallel formations

- phenyl groups contain additional conjugated π-electron systems
  - hydrophobic
  - these groups alone should not lead to the stacking due to dispersive interactions, because of the size of the molecules and TEG chains acting as sterical barriers

- it is *artificial* and to the best of our knowledge it never existed on this planet. That means that until recently, there was no empirically supported precedent as to how **3,4,5-TEG-TPP** could be expected to behave, for example how toxic it is.
  - there is likely much research to be done

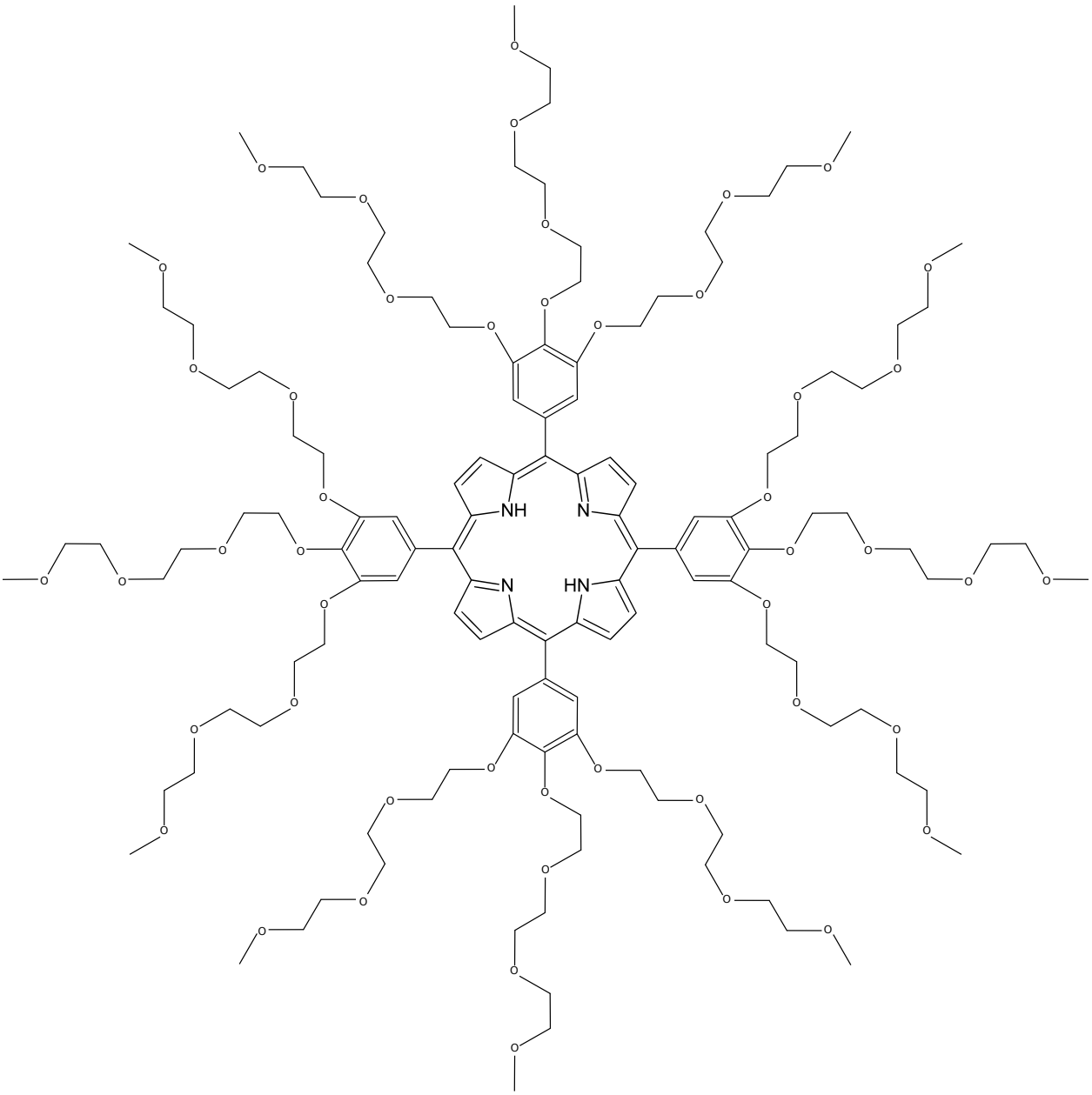

Figure 1.4: **3,4,5-TEG-TPP** ("tetraphenylated porphyrin with tetraethylene glycol-like side chains at phenyl sites 3, 4 and 5"), the porphyrin of our interest. Owing to the tetraethylene glycol-like side chains, this porphyrin has a relatively good solubility and also undergoes phase separation with lower critical solution temperature at around 50°C.

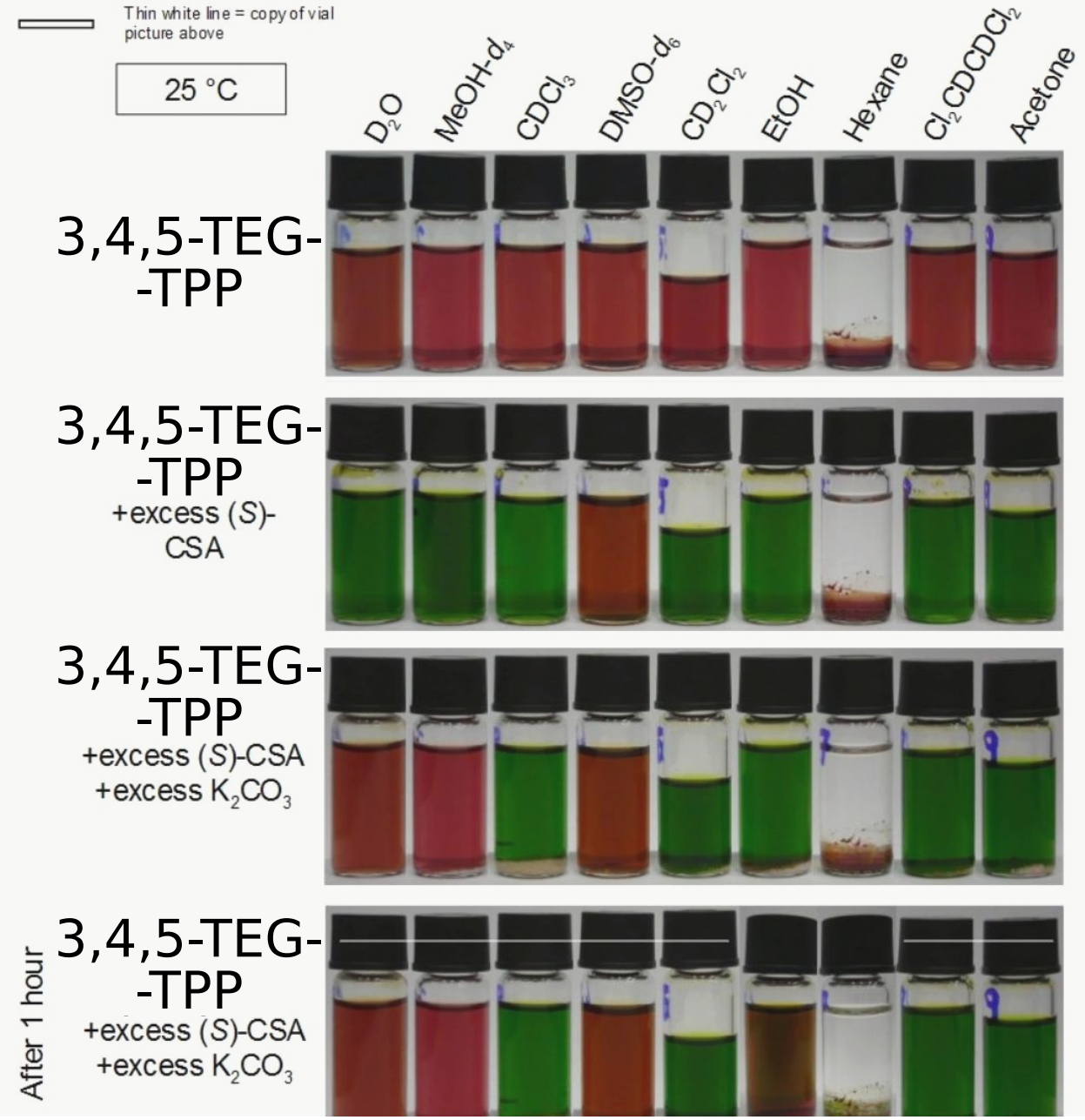

Figure 1.5: **3,4,5-TEG-TPP** dissolved in various solvents. The substance is dark brownred and oil-like when pure, insoluble in hexane and its solutions are also brownred, each with a different tint. The addition of *S*-camphorsulfonic acid leads to complexation of free protons with the **3,4,5-TEG-TPP** molecules. This changes the energy spectrum of the conjugated macrocycle which can be seen as the color shift to green. In D_2O, MeOH and EtOH this can be reversed by adding a base that neutralizes the free protons dissociated from *S*-CSA.

1.4 Motivation

The compound **3,4,5-TEG-TPP** has a few properties that make it interesting, special, and possibly useful:

- possible aplications:
  - reusable agents for selective separation of ligands from solution (using the complexation and phase separation properties)
  - solubilization of carbon nano-tubes
  - sensing of:
    - enantiomeric excess; chiral active ingredients in medicine and food industry are commonplace[1]
    - pH, even in non-aqueous solutions, for which no litmus papers exist
    - temperature
  - catalysts/functional pigments
- it shares some properties with compounds of utmost importance for life on Earth, e.g. the porphyrins heme, chlorophyll and vitamin B_{12}:
  - complexation capabilities
  - absorption in the visible spectrum
  - solvatochromism
- it has a new, potentially radical property – it is *soluble in water*. Unlike heme for example, it needs no protein to bind to for the purpose of directed transport.
- it differs from other, especially simple porphyrins – the TEG-like chains function as sterical barriers that restrict the possibility of dispersive interaction stacking to some degree[2].

How do these properties and effects affect each other? How much? What possible applications and further research suggestions are there?

1.5 Goals of this thesis

The goals of this diploma thesis are to study the temperature-responsive properties of **3,4,5-TEG-TPP**. The properties of interest that we have finalized experimental results for, are:

- quantify the *phase separation* occuring at around 320 K, with regards to solution temperature and composition.
- apply the Flory-Huggins theory of polymer solutions to find the *binodal* and *spinodal* of phase separation (i.e. construct temperature-composition *phase diagram*)
- examine *how acid complexation affects* the other supramolecular interactions of **3,4,5-TEG-TPP**
- draw qualitative conclusions about the behavior of **3,4,5-TEG-TPP** in aqueous solution – how its molecules interact with each other and with acid – supported by experimental results. What has been achieved by performing this chemical modification?

[1] For example menthol [17], bupivacaine [18], carvone [**?**], thalidomide [19] and monosodium glutamate [20].

[2] When two **3,4,5-TEG-TPP** molecules stack, the chains will have a reduced set of random conformations to adopt. Our results seem to imply that for two molecules this entropic penalty is not significant, but it is prohibitive for 3+ molecular stacks. This is according to our results both with and without acid in the solution; the r parameter value implies reliable formation of dimers, see the Figure 4.13, the stoichiometry of H^+ formation and existence of a limited set of transitory complexes, see the Figure 4.17, and implies the "sandwich" model in the Figure 4.19.

2. Methods

Now that we have established the context, object, importance and goals of our research, we must present the main sources of tools that are used to arrive at the results (these methods will be adapted to our particular problem in the next chapter, the Definitions of Observables 3):

- the experimental method called Nuclear Magnetic Resonance spectroscopy is used to acquire the data. This includes the proof of molecular structure in the Figure 1.4, phase separation quantification and interaction with acid.
- the Flory-Huggins Liquid Lattice Theory of Polymer Solutions used to interpret the phase separation data and arrive at a phase diagram. The Gibbs energy of mixing for the porphyrin and solvent derived in a mean field approximation and phase equilibrium conditions used to derive the ways to find the binodal and spinodal of the phase separation.

2.1 Nuclear Magnetic Resonance

Nuclear magnetic resonance spectroscopy (NMR) is an experimental method of condensed matter physics. It uses very large stationary magnetic fields (in the order of 10 T) to induce *observable nuclear magnetization* in samples that are *diamagnets or paramagnets* in terms of electron magnetization. When we create non-zero quantum coherences in nuclear spin states by radio-frequency pulse excitation, nuclei will radiate radio-freqency signal with *frequency accurately dependent on the local magnetic fields in each nucleus*, before relaxing to equilibrium. We measure and process this signal into spectra. The *local magnetic fields change with the chemical environment of the nucleus* – both in mean value and temporal self-correlation. Thus we can experimentally prove bonds, changes in molecular behavior or conformation, chemical exchange, and measure correlations in signal from various nuclei – and *prove the molecular structure* of given sample. In most experiments – depending on the excitation and acquisition procedure – signal is proportional to the number of nuclei in a given chemical environment. This means that we can also *determine chemical composition quantitatively* – relative to a standard or other chemical components.

As for NMR literature, I recommend Malcolm H. Levitt's *Spin Dynamics* [21] and Harald Gunther's *NMR Spectroscopy* [22].

2.1.1 NMR experiments

Assume that a NMR sample is in thermodynamic equilibrium and ready for the experiment. In the NMR terminology a *pulse sequence* is what we subject the sample to before the signal comes out and can be processed. A pulse sequence can contain one or more radio-frequency pulses, each with some given intensity profile and duration. Some pulses are used to manipulate the populations and coherences of the spin density matrix directly (sometimes selectively), some are used to decouple interactions between nuclei, some are used to induce magnetic field gradients. The type of experiment is fundamentally dictated by the pulse sequences used, but it can also consist of a set of experiments where some parameter other than pulse sequence changes. In this section we explain the most basic $\frac{\pi}{2}$ pulse experiment, the *variable temperature series* and the *titration* measurements. The latter two are sets of simple *1D spectra*.

$\frac{\pi}{2}$ pulse 1D spectrum

The simplest and most commonly used pulse sequence in the NMR method contains a single, $\frac{\pi}{2}$ *pulse*. A "$\frac{\pi}{2}$ pulse" is one with an ideally tooth-like intensity and a duration such that: duration times nutation equals $\frac{\pi}{2}$ radians. Such a pulse creates the largest possible value of spin coherences for the given isotope. Immediately after the dead time of the RF coil, FID is measured. Transformation of the FID results in a *1D spectrum*. The spectrum is one-dimensional in the sense that the pulse sequence contains *precisely one time axis* which characterizes when the detector readout was taken by the computer. This axis is the *time axis of the FID*[1].

[1]When relevant, additional axes are additional *delay parameters between pulses* of more complicated pulse sequeces, or the *numbers of repetitions of a segment* of a pulse sequence; "variable delay" (VD) and "variable count" (VC) respectively.

Such a simple and quick 1D spectrum already contains a lot of useful information. We can often estimate whether the sample is really what it should be, and whether we can continue with other measurements or what parameters/procedures we have to refine/use to improve the signal first. Peak areas are proportional to the number of nuclei at given sites. Although other measurements may be necassary to assign the peaks to sites, 1D peak assignment is always a useful key for decoding the results of further measurements. Identifying the signals lets us interpret multidimensional correlation spectra and use the proportionality of signals to measure the composition and phase-separated porphyrin fraction of the sample.

Variable Temperature (VT) series

A set of 1D spectra measured for the same sample with the only change between measurements being the *sample temperature* is called a *variable temperature series* (VT series). VT series are useful for quantifying temperature-dependent phenomenona. One of our goals is to quantify the phase sepratation of **3,4,5-TEG-TPP** with respect to its volume fraction and temperature. Given these facts, the optimal algorithm for achieving our goal is:

1. prepare a very concentrated, almost saturated solution
2. measure the first VT series[2]
3. dilute the sample somewhat[3], remove some of the solution if necessary
4. measure the second VT series
5. dilute the sample somewhat, remove some of the solution if necessary
6. ...

Titration

Analogously to the VT series, a *titration* measurement is a set of 1D experiments for the same sample, with the only change being that we add some other chemical compound (in our case *S*-camphorsulfonic acid) to the mixture with the intention to observe and quantify the interaction of the components. If the components do not interact in any specific way, the resulting spectrum will be a simple sum of the spectra of separate components. If the components affect each other, we can observe various changes including peak shifts or width changes, peak splitting, chemical exchange between various complexes or a change in the temperature dependence of phase separation.

Multidimensional experiments require large numbers of near-identical scans to be done; a few for each possible combination of parameters.

[2]It is expedient to choose a distribution of temperatures which is dense where we expect the non-trivial region of the phenomenon to lie. E.g. for phase separation measurements in the region where the sigmoid curve has bends or a slope.

[3]It makes sense to choose a geometrical series of concentrations in order to distribute them equidistantly on a logarithmic axis, due to logarithmic plots being useful in the low concentration region. See the second plot in the Figure 4.13.

2.2 Flory-Huggins Liquid Lattice Theory

Since one of the goals of this work is to apply the Flory-Huggins theory of polymer solutions to the aqueous solutions of **3,4,5-TEG-TPP** and construct the binodal and spinodal curves which together describe the phase equilibrium of the solution, the objective of this section is to present:

- the expression for mixing Gibbs energy of a star-like polymer solution ΔG_{mix}, the Equation 2.1
- a pair of equations that we can use to fit the binodal curve to experimental datapoints; the Equations 2.3 and 2.4
- an equation that we can use to find the spinodal curve, the Equation 2.16. Note: We cannot measure the spinodal using NMR, spinodal will only be calculated using the results of binodal fitting.

The following sections contain the main points from the Paul J. Flory's book, Principles of Polymer Chemistry[23], taken from the chapter *12. Statistical Thermodynamics of Polymer Solutions* and the chapter *13. Phase Equilibria in Polymer Systems.*

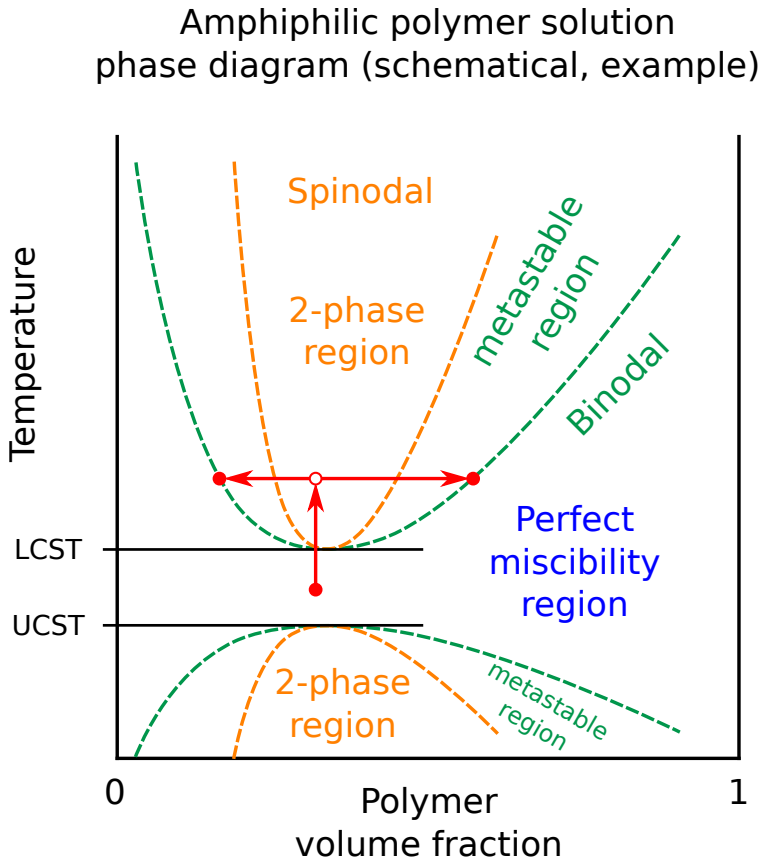

Figure 2.1: Example of a fictional amphiphilic polymer's phase diagram - an illustration of the upper and lower critical solution temperatures [24]. The aim of the Flory-Huggins Liquid Lattice Theory section is to substantiate such a phase diagram theoretically and to derive ways of finding (Section 3.4) the binodal (the Equations 2.3, 2.4) and spinodal (the Equation 2.16) curves when applied to our experimental data in the Chapter 4. Polymer/porphyrin volume fraction is denoted by ϕ_2 in the Flory-Huggins theory and ϕ_P when referring to our application of this theory.

2.2.1 Gibbs energy of mixing

In the previous two sections, we derived both the quantities ΔH_{mix} and ΔS_{mix} needed to define the *Gibbs energy of mixing*. We use the general definition

$$G = H - TS$$

and substitute the equations for enthalpy and entropy derived from the liquid lattice theory into $\Delta G_{mix} = \Delta H_{mix} - T\Delta S_{mix}$ to obtain

$$\Delta G_{mix} = n_0 k_B T \left[\phi_1 \ln \phi_1 + \frac{\phi_2}{r} \ln \phi_2 + \chi \phi_1 \phi_2 \right]. \tag{2.1}$$

Since the volume fractions are bound by the inherent constraint $\phi_1 + \phi_P = 1$, a more appropriate version of the Equation 2.1 above will be used:

$$\Delta G_{mix}(T, \phi_P) = n_0 k_B T \left[(1 - \phi_P) \ln (1 - \phi_P) + \frac{\phi_P}{r} \ln \phi_P + \chi (1 - \phi_P) \phi_P \right]. \tag{2.2}$$

2.2.2 Phase equilibrium (binodal and spinodal)

The solution – as any thermodynamic system – will over time adopt a state in which there is a phase equilibrium. The equilibrium state of our system is characterized by a pair of thermodynamical parameters, the temperature and composition (T, ϕ_2); we chose the volume fraction of porphyrin to describe the composition. We always assume the pressure to be constant. There can be one or more phases:

- when there is only one phase, we say that the chemical components are *perfectly miscible*. This happens when the interations between unlike species [1, 2] are preferred as opposed to interactions between like species [1, 1], [2, 2]; and even when these interactions are not preferred but the entropy penalty of coagulation at given (T, ϕ_2) is sufficient to counteract the phase separation.
- when there is a *solvent-rich* and a *porphyrin-rich* phase, we say that the solution underwent *phase separation*. This happens when the mixing entropy is not sufficient to keep the solvophobic porphyrin molecules apart. In principle, both temperature increase and temperature decrease can cause this phenomenon.

The depiction of the set of all possible values of (T, ϕ_2) together with the boundary curve between the perfect miscibility and phase separation regions is called a *temperature-comopsition phase diagram of a binary solution*. The curve separating these regions is called the *binodal curve*. An example of such a phase diagram is in the Figure 2.1 and the resulting phase diagram of this thesis for the molecule **3,4,5-TEG-TPP** is in the Figure 4.13.

As was mentioned, the phase sepration can in principle be produced both by temperature increase and temperature decrease. The lowest or highest temperature when this can happen, for any possible composition is called *lower critical solution temperature* and *upper critical solution temperature*, respectively, commonly abbreviated as LCST and UCST. The meaning of these quantities is readily understood from the Figure 2.1.

Let us assume there can exist two different phases[4] – let us call them the solvent-rich α phase and the porphyrin-rich β phase – at given temperature and composition. In each of those phases the volume fraction of compound 1 and 2 is different. Thus we introduce the quantities $\phi_1^\alpha, \phi_2^\alpha, \phi_1^\beta, \phi_2^\beta$. These are illustrated in the Figure 4.12.

The phase equilibrium is defined as the state where no further observable relaxation of chemical composition can occur. This happens when the *chemical potentials* of each of the chemical components are equal among all possible phases, because at that point no particular phase transition is preferred and some dynamic equilibrium is established, in our case:

[4]... as is apparent from optical microscopy, see the Figure 4.26. My supervisor also did supporting optical microscopy experiments, see the section 4.5

$$\mu_1^\alpha = \mu_1^\beta \tag{2.3}$$
$$\mu_2^\alpha = \mu_2^\beta \tag{2.4}$$

The chemical potentials above are defined as

$$\mu_1^\alpha = \partial_{\phi_1^\alpha} \Delta G_{mix}^\alpha(T, \phi_1^\alpha) \tag{2.5}$$
$$\mu_1^\beta = \partial_{\phi_1^\beta} \Delta G_{mix}^\beta(T, \phi_1^\beta) \tag{2.6}$$
$$\mu_2^\alpha = \partial_{\phi_2^\alpha} \Delta G_{mix}^\alpha(T, \phi_2^\alpha) \tag{2.7}$$
$$\mu_2^\beta = \partial_{\phi_2^\beta} \Delta G_{mix}^\beta(T, \phi_2^\beta). \tag{2.8}$$

It needs to be noted explicitly that the derivatives in composition need to be thought of as local fluctuations of porphyrin density, since the porphyrin is not appearing in or disappearing from the solution, and that it would be more appropriate to think of the Gibbs energy as the density of the Gibbs energy dependent on that local fluctuating composition; possibly added up over all subsystems.

Using the definitions of chemical potentials above, the two phase equilibrium conditions, the Equations 2.3 and 2.4 above can be expressed as the two functions – f_1, f_2 – to be numerically minimized below:

$$f_1 = 0 = \ln(1-\phi_2^\alpha) - \ln(1-\phi_2^\beta) + \left(1 - \frac{1}{r}\right)\left(\phi_2^\alpha - \phi_2^\beta\right) + \chi\left[(\phi_2^\alpha)^2 - (\phi_2^\beta)^2\right] \tag{2.9}$$
$$f_2 = 0 = \ln(\phi_2^\alpha) - \ln(\phi_2^\beta) - (1-r)\left(\phi_2^\alpha - \phi_2^\beta\right) + \chi\left[(1-\phi_2^\alpha)^2 - (1-\phi_2^\beta)^2\right] \tag{2.10}$$

In the equations above there are seemingly four variables: $\phi_2^\alpha, \phi_2^\beta, r, \chi$; χ remaining conspicuously undefined. Without introducing too many unnecessary degrees of freedom, we will assume the form of interaction parameter χ to be

$$\chi(T; A, B) := A + \frac{B}{T}. \tag{2.11}$$

The values A, B are related to the mixing enthalpy and entropy, however their values cannot be interpreted in a straightforward fashion.

The system of Equations 2.9 and 2.10 is the condition that we will use to find the *binodal curve*. The search for the binodal involves six variables – minus two constraints (equations for $\phi_2^\alpha, \phi_2^\beta$ equilibria) minus one parameter (ϕ_P) which will necessarily remain free to parametrize the binodal curve ($\phi_P, T(\phi_P)$) – there remain three parameters that together define the binodal uniquely: (r, A, B).

If we heat up the solution while it is in a state of perfect miscibility and force it to cross the binodal into the region of *meta-stability* of the phase diagram, it can start to decompose into a continuum of phases provided some local fluctuations/disturbances. However, in principle, the decomposition *does not necessarily occur* by itself. If we consider the thermodynamic stability of the solution with respect to *infinitesimal disturbances*, we arrive at the inequality

$$\partial_{\phi_P \phi_P} \Delta G_{mix}(T, \phi_P) > 0. \tag{2.12}$$

If the local composition fluctuates slightly, the Gibbs energy increases, i.e. *entropy decreases*. That means a deviation from the equilibrium. That means that additional fluctuations acting as a "returning force" for the system back towards the equilibrium *become more likely* – the current state is *locally stable*. On the other hand if the Gibbs energy decreases due to infinitesimal fluctuations – which implies an *increase in entropy* – such fluctuations are more likely than "returning fluctuations" and the system is being propelled into some significantly different state – the current one is *unstable*. The set of points separating these regions – where the inequality 2.12 is an exact equality – is called the *spinodal curve*. It is thermodynamically *impossible* to maintain a homogeneous system with (ϕ_P, T) inside the spinodal curve – the system *spontaneously separates*

into several phases, all of which are outside the spinodal and under external stimuli and fluctuations *tend towards the binodal*. The whole-system-average (ϕ_P, T) will stay inside the spinodal region, however. Thus we can write the condition for points belonging to the spinodal as:

$$\partial_{\phi_P \phi_P} \Delta G_{mix}(T, \phi_P) = 0 \tag{2.13}$$

The explicit form of $\Delta G_{mix}(T, \phi_P)$ being

$$\Delta G_{mix}(T, P, \phi_P) = n_0 k_B T \left[(1 - \phi_P) \ln (1 - \phi_P) + \frac{\phi_P}{r} \ln \phi_P + \chi (1 - \phi_P) \phi_P \right], \tag{2.14}$$

the definition of the spinodal 2.13 above translates into the equation

$$\chi = \frac{1}{2} \left(\frac{1}{r \phi_P} + \frac{1}{1 - \phi_P} \right). \tag{2.15}$$

After plugging in the assumed form of the interaction parameter χ in the Equation 2.11, we can express the spinodal curve as the set of (ϕ_P, T) points for which the following relation holds:

$$T = \frac{B}{\frac{1}{2} \left(\frac{1}{r \phi_P} + \frac{1}{1 - \phi_P} \right) - A}. \tag{2.16}$$

To plot this curve, we need to arrive at some collection of parameters (r, A, B) describing our particular system and its phase diagram first. The Section 3.4 explains how we did this for the molecule **3,4,5-TEG-TPP**. How both the binodal and spinodal turned out with respect to experimental data can be seen in the Figure 4.13.

3. Definitions of Observables

Before measuring anything, showing results and drawing conclusions, it is necessary to formulate *what exactly* we are going to observe and why it makes sense to do so. We have already explained what our goals and reasons for pursuing them are in the Sections 1.5 and 1.4. That means that the abstract needs have been formulated. Now we need to somehow connect the world of our ideas and needs with objective physical reality – i.e. the phenomena to be observed in experiment. To do precisely that, we need to introduce mathematical objects which serve to describe the object of our study in terms of measurable quantities well established in physics and chemistry.

3.1 Theoretical phase-separated fraction – f_{sep}

The first such object is *phase-separated fraction*, from now on denoted f_{sep}.

We assume that each porphyrin molecule in solution can be found in exactly one of two discrete states. The states are *phase-separated* and *non-phase-separated*, each characterized by an instantaneous value of molar concentration $[P_{nsep}]$ and $[P_{sep}]$. We also assume that both of these states have well-defined molar enthalpies and molar entropies, $h_{nsep}, h_{sep}, s_{nsep}, s_{sep}$ respectively; but only the differences of these quantities between states, $\Delta h = h_{sep} - h_{nsep}, \quad \Delta s = s_{sep} - s_{nsep}$, are relevant to the dynamics of the porphyrin solution; we also assume that the enthalpy and entropy differences $\Delta h, \Delta s$ are constant for any fixed total porphyrin concentration. Both of the assumptions are somewhat dubious – as the *local* concentration of porphyrin in each phase will change with temperature and the values have to depend on *local* properties of the solution – but as we are going to see later in an example of experimental data – the Figure 4.11 – the assumption is good enough and not harmful to our goals.

It needs to be stressed that although there *might* be some obscure relation between the molar enthalpies and entropies in the paragraph above and the enthalpies and entropies discussed in the Section 2.2, these quantities are not nearly the same thing. The quantities in the previous chapter quantified the Gibbs energy differences between completely pure and abitrarily mixed solutions. The quantities used in this section quantify the average desirability for porphyrin molecules to transition from a perfect mixture into the porphyrin-rich β phase, gradually impoverishing the solution of well-dissolved porphyrin turning it into the solvent-rich α phase in the process.

The phase-separated fraction is thus a function of temperature and has two parameters, $(\Delta h, \Delta s)$ which are in truth dependent on concentration of porphyrin in solution, but we make no assumptions as to how exactly. Using these two quantities, we define the difference of molar Gibbs energies between the states and express the *equilibrium constant* K, Equations 3.1 and 3.2.

$$\Delta g = \Delta h - T\Delta s \tag{3.1}$$

$$K = \frac{[P_{sep}]}{[P_{nsep}]} = \mathrm{e}^{-\frac{\Delta g}{RT}} = \mathrm{e}^{-\frac{\Delta G}{nRT}} \tag{3.2}$$

Finally, we define f_{sep} as the ratio of phase-separated porphyrin concentration to the total concentration of porphyrin in the solution, Equation 3.4 below. All of the quantities and the whole process is depicted in the Figure 3.1.

$$f_{sep} := \frac{[P_{sep}]}{[P_{sep}] + [P_{nsep}]} = \frac{1}{1 + \frac{1}{K}} \tag{3.3}$$

$$= \frac{1}{1 + \mathrm{e}^{\frac{\Delta h}{RT} - \frac{\Delta s}{R}}} \tag{3.4}$$

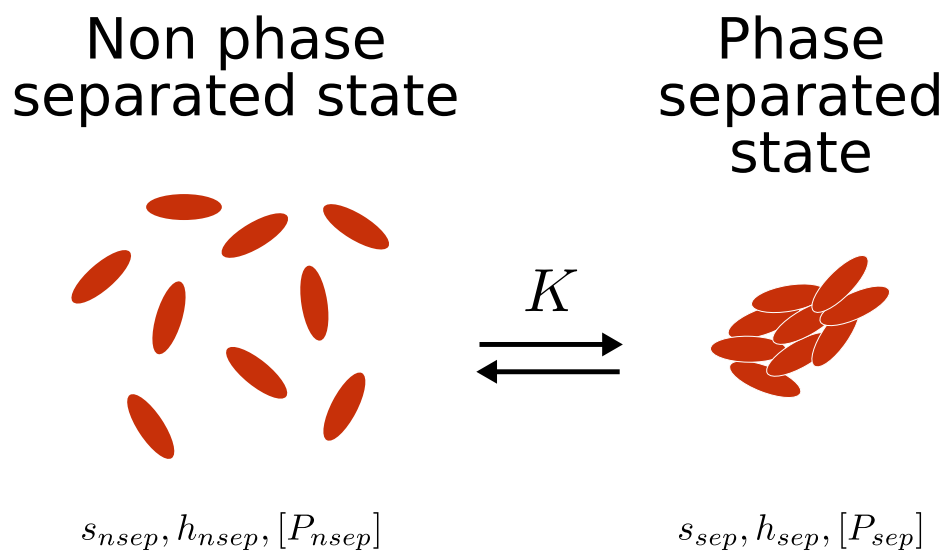

$$\Delta h = h_{sep} - h_{nsep}, \quad \Delta s = s_{sep} - s_{nsep}$$

$$\Delta g = \Delta h - T\Delta s$$

$$K = \frac{[P_{sep}]}{[P_{nsep}]} = \mathrm{e}^{-\frac{\Delta g}{RT}} = \mathrm{e}^{-\frac{\Delta G}{NRT}}$$

$$f_{sep} := \frac{[P_{sep}]}{[P_{sep}]+[P_{nsep}]} = \frac{1}{1+\frac{1}{K}}$$

$$\boxed{f_{sep} = \frac{1}{1+\mathrm{e}^{\frac{\Delta h}{RT} - \frac{\Delta s}{R}}}}$$

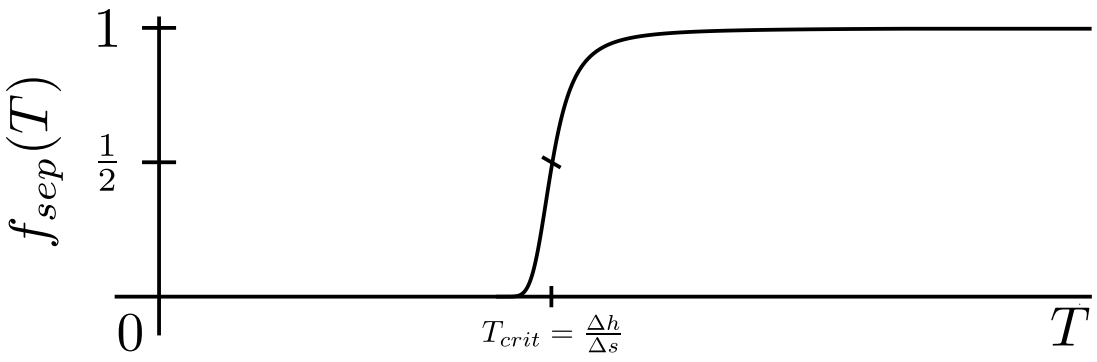

Figure 3.1: We assume that **3,4,5-TEG-TPP** molecules can occupy exactly two states - they can either be phase-separated or not. Each of those states has a molar enthalpy, entropy and a concentration. We use these quantities to define the equilibrium constant K. f_{sep} – the phase-separated fraction is then a function of temperature and two parameters – molar enthalpies and entropies $(\Delta h, \Delta s)$ – to be found by fitting experimental data later.

3.2 Experimental phase-separated fraction – f_{sep}

Now that the theoretical f_{sep} has been defined, we should explain how do we acquire it experimentally.

To measure f_{sep}, the simplest 1D pulse sequence mentioned at the beginning of the Subsection 2.1.1 is used. We acquire a 1D spectrum and measure the ratio of certain signals the area of which quantifies *all porphyrin* to certain signals that quantify the *phase-separated porphyrin*, exactly as the theoretical definition of f_{sep} says. This is done by identifying the signals and fitting/integrating them. The Figure 3.2 shows the site naming and the rationale in establishing the Equation 3.5.

The number of C-sites in one fourth of the molecule is 6. The number of A-type and B-type sites is 2 each. The signals for these sites in molecules that underwent phase separation are called C', A' and B' respectively. If we can measure areas of these peaks, we should be able to calculate the f_{sep} in terms of these areas. It turns out that measuring the ratio of C' area to the sum of areas of A, A', B, B' is the most viable way.

Assuming that all porphyrin separates at high temperatures, asymptotically the experimental value of f_{sep} should tend towards 1. However, we know that the ratio of C' nuclei to A+A'+B+B' nuclei would be 6 to 4. Thus we have to normalize the relation, giving rise to the Equation 3.5:

$$f_{sep} = \frac{4}{6}\frac{C'}{A + A' + B + B'} \tag{3.5}$$

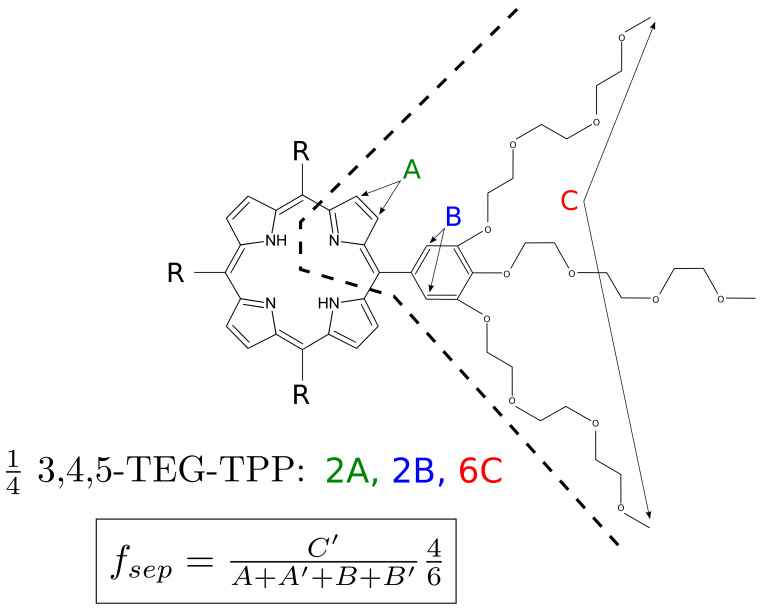

Figure 3.2: The site naming for f_{sep} quantification. Each spectrum of a VT series at given ϕ_P has a f_{sep} that we calculate as a ratio of peak areas. We fit peaks of sites A, B (and their separated counterparts A', B' if necessary) and the peak C' using Lorentzian curves in low ϕ_P spectra and pseudo-Voigt curves at higher ϕ_P. The ratio of hydrogens at site C to hydrogens at A and B in one fourth of a **3,4,5-TEG-TPP** molecule is 6:4. From high temperature limit considerations we deduce the need to normalize f_{sep} by multiplying it by "$\frac{4}{6}$".

3.3 Onset temperature of phase separation – T_{ONSET}

To acquire the tuple (r, A, B), we need to fit the theory to experimental points. Each of the measured VT series and its f_{sep} function have to be reduced to a single temperature point where the phase separation starts to occur. Such a point will be called T_{ONSET}, and is defined in the next paragraph and elucidated by the construction shown in Figure 3.3.

The $f_{sep}(T; \Delta h, \Delta s)$ function has an inflex point in T dependent on the $(\Delta h, \Delta s)$ parameters. We calculate the tangent line at the inflex point. The intercept of the tangent and $f_{sep} = 0$ is at the temperature T_{ONSET}. Unfortunately, neither the T_{INF} nor T_{ONSET} can be given explicitly in terms of $(\Delta h, \Delta s)$, as they are defined as a solution of a transcendental equation or a function thereof, respectively. It is necessary to first numerically calculate the temperature of the inflex point T_{INF}, then the f_{sep} and its first derivative; finally evaluate the Equation 3.10. The relations used in this construction are shown below:

$$f_{sep}(T; \Delta h, \Delta s) = \frac{1}{1 + \mathrm{e}^{\frac{\Delta \mathrm{h}}{\mathrm{RT}} - \frac{\Delta \mathrm{s}}{\mathrm{R}}}} \tag{3.6}$$

$$\frac{\mathrm{df_{sep}}}{\mathrm{dT}}(T; \Delta h, \Delta s) = \frac{\Delta h}{2RT^2} \frac{1}{\cosh(\frac{\Delta h}{RT} - \frac{\Delta s}{R}) + 1} \tag{3.7}$$

$$\frac{\mathrm{d^2f_{sep}}}{\mathrm{dT^2}}(T; \Delta h, \Delta s) = \frac{\Delta h}{2RT^2} \frac{\left[\frac{\Delta h}{RT^2} \tanh\left(\frac{\Delta h}{2RT} - \frac{\Delta s}{2R}\right) - \frac{2}{T}\right]}{\cosh(\frac{\Delta h}{RT} - \frac{\Delta s}{R}) + 1} \tag{3.8}$$

$$T_{INF}: \quad \frac{\mathrm{d^2f_{sep}}}{\mathrm{dT^2}}(T_{INF}; \Delta h, \Delta s) = 0 \iff \frac{\Delta h}{RT_{INF}^2} \tanh\left(\frac{\Delta h}{2RT_{INF}} - \frac{\Delta s}{2R}\right) = \frac{2}{T_{INF}} \tag{3.9}$$

$$T_{ONSET} := T_{INF} - \frac{f_{sep}(T_{INF})}{f'_{sep}(T_{INF})} \tag{3.10}$$

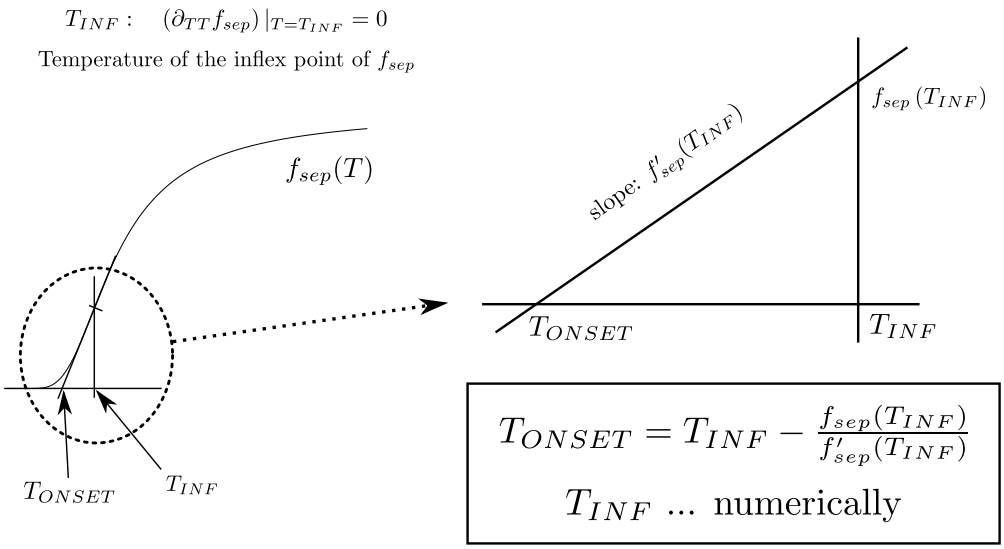

T_{ONSET} is the most important quantity to be determined here!

Figure 3.3: The determination of T_{ONSET} for a given VT series with fixed porphyrin volume fraction ϕ_P. For equations and procedures involved, refer to Equations 3.6–3.10 and the points right above this Figure.

3.4 Phase diagram

When we mention *phase diagram*, we will always talk about the *temperature-composition* plot of the binodal and spinodal curves of the molecule **3,4,5-TEG-TPP**, i.e. the two sets of (ϕ_P, T) for which the system of Equations 2.9 and 2.10 holds true, and Equation 2.16 holds. Both of these curves are uniquely given by the tuple of parameters (r, A, B). For this reason, from the perspective of research goals knowing the phase diagram is equivalent with finding (r, A, B) for the aqueous solution of **3,4,5-TEG-TPP**.

What we have achieved in Subsection 2.2.2 is that now we are *in principle* able to *fit the binodal curve* to any set of *experimental points* (T, ϕ_P). That way we arrive at the experimentally supported (r, A, B).

To solve the system of equations, i.e. minimize the functions f_1 in the Equation 2.9 and the function f_2 in Equation 2.10 we implemented the two-dimensional Newton method. This way we calculate a binodal that we then compare with the experimental data. The whole fitting procedure is described below:

1. guess/refine (r, A, B)
2. Newton's method for each of the experimental ϕ_2^α:
   (a) ϕ_2^α is a fixed parameter; we know what **3,4,5-TEG-TPP** concentration we prepared the sample with
   (b) ϕ_2^β, χ are treated as the variables of the system of equations[1]
   (c) the Jacobian is calculated with respect to ϕ_2^β, χ and the tangent intersection with zero estimated a number of times
   (d) we acquire some new value of χ
3. $T(\chi; A, B)$ are calculated and compared with each of their corresponding experimental T_{ONSET} values
4. repeat from point 1 until satisfactory (r, A, B) is found

The process of solving the set of equations is rather unstable. We strongly recommend the following constraints for the search to have a chance to converge:

- $10^{-6} < \phi_2^\alpha < \phi^{crit} = \frac{1}{1+\sqrt{r}} < \phi_2^\beta < 1 - 10^{-6}$
- $\chi > \chi^{crit} = \frac{1}{2}\left(1 + \frac{1}{\sqrt{r}}\right)^2$

The critical values ϕ^{crit}, χ^{crit} are the volume fraction and the interaction parameter $\chi^{crit} := \chi(LCST; A, B)$ (calculated using to the Equation 2.11) which are equivalent with the coordinates of the binodal minumum in Figure 2.1. It is handy to calculate the approximate r value beforehand if the binodal minimum can be estimated.

Once the true values of (r, A, B) are known, Flory-Huggins theory also gives us a way to calculate the LCST from the χ^{crit} above as

$$LCST = \frac{B}{\chi^{crit} - A} = \frac{B}{\frac{1}{2}\left(1 + \frac{1}{\sqrt{r}}\right)^2 - A} \tag{3.11}$$

and ϕ_P^{crit} at which LCST can be found is given by

$$\phi_P^{crit} = \phi^{crit} = \frac{1}{1+\sqrt{r}}. \tag{3.12}$$

[1] ϕ_2^β is freely manipulated to find ϕ_2^α, but we discard it afterwards because it is of no use. However, for a few points past ϕ_{crit}, the roles of ϕ_2^α and ϕ_2^β are reversed.

4. Results and Discussion

In this chapter we present three kinds of information:

1. what sets of experiments we performed
2. how we processed the data
3. the results we acquired by processing the experimental data

The data acquired is interpreted according to the NMR and Flory-Huggins Liquid Lattice theories, both explained in Chapter 2. The quantities and objects observed were introduced and rationale used in defining them explained in the Chapter 3.

As for the topics of this chapter, we need to:

1. provide the rationale for believing that the sample contains molecules shown in the Figure 1.4, this is done in Section 4.1
2. summarize how we processed the data and show the results on the temperature-dependent behavior in the Section 4.2; the methods used have already been discussed in the Chapter 3
3. show and interpret the data from acid titration measurements, the Section 4.3

4.1 Structural proof and peak assignment experiments

As has been mentioned, when starting experiments it is important to verify whether the substance we are handed is *really* what we are told it is. Otherwise we might find ourselves working for years in vain. In this section we present peak assignment 1D spectra of the compound **3,4,5-TEG-TPP** and some 2D correlation measurements we did in order to support the assertion that our samples contain the molecule from the Figure 1.4.

^{1}H peak assignment

As the first step of the peak assignment, we have to name the chemical sites at which the observed isotopes are located. The ^{1}H site naming is shown in the Figure 4.1. Then ^{1}H 1D spectra were measured in D_2O and $CDCl_3$ – the Figures 4.2 and 4.3 follow. The peaks of the aliphatic region are resolved to a much higher degree in $CDCl_3$ than in D_2O. The Figure 4.4 shows the detailed aliphatic region peak assignment. The aliphatic region consists of six pairs of triplet-like multiplets. In each of the six pairs, one of the multiplets always has double the peak area compared to the other since there are two TEG-like side chains for each central TEG-like chain[1]. The chemical shifts of the peaks are explained by the ring current effect. Both the tetrapyrrolic macrocycle and the phenyls are diamagnetic electron densities causing nearby in-plane ^{1}H sites to shift to the left. As the distance from these rings increases, the chemical shift also decreases. This trend is actually the dominant chemical shift-influencing effect across the whole spectrum, both in D_2O and $CDCl_3$. The only exception is the E peak in at chemical shift -3 ppm in $CDCl_3$. The reason for this exotic chemical shift is that the hydrogen is located near the center of the ring, where the ring current effect is negative. The E peak cannot be seen in D_2O, as the hydrogen is chemically exchanged with the solvent and practically all of those E hydrogen sites are in fact occupied by deuteria – which are not visible in ^{1}H experiments.

[1] The ^{1}H on the methyl end groups of the TEG-like side chains are chemically equivalent due to the symmetry of the **3,4,5-TEG-TPP** molecules.

3,4,5-TEG-TPP site naming for ^{1}H peak assignment

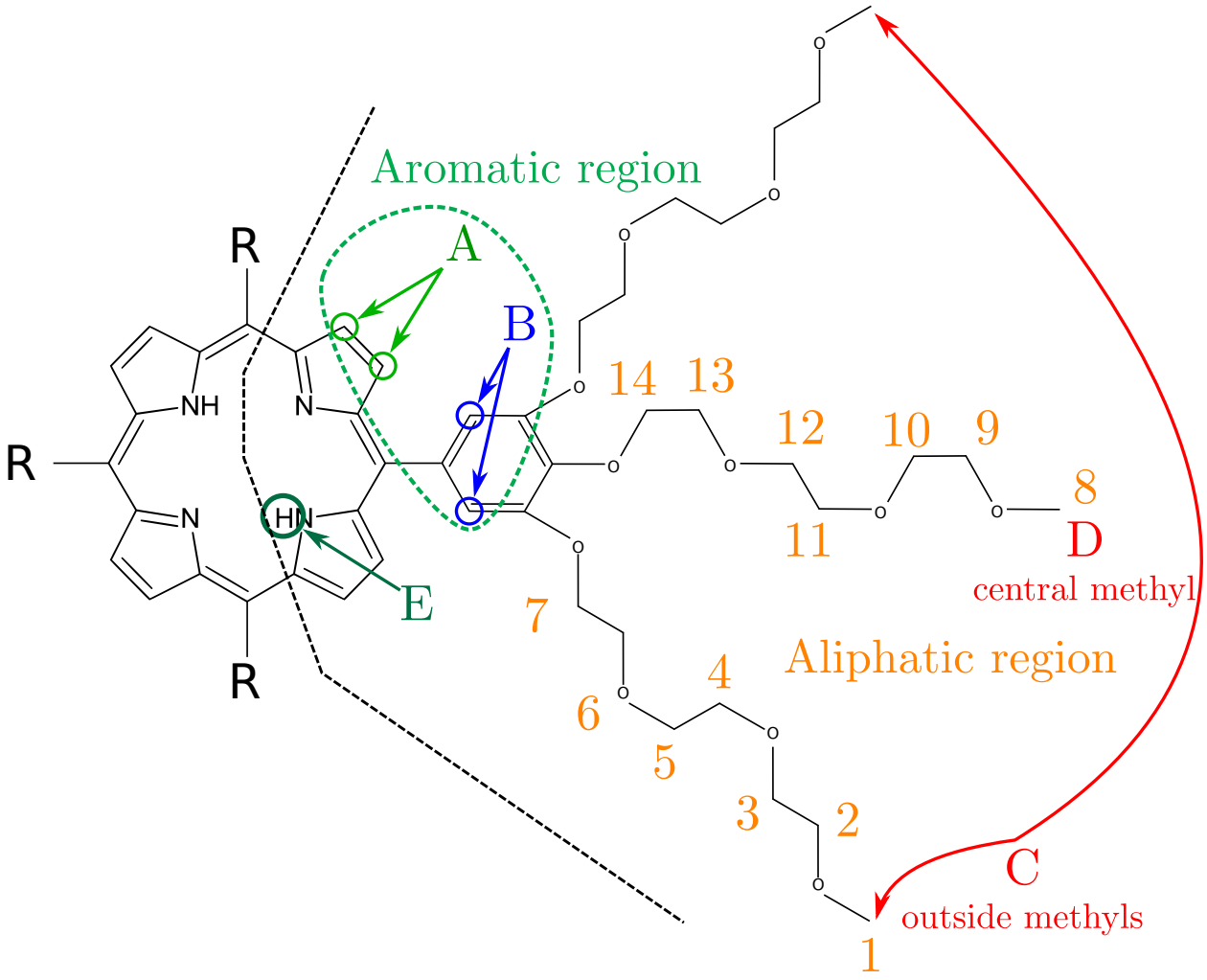

Figure 4.1: Site naming for the ^{1}H peak assignment. The letter "R" stands for the other three 3,4,5-TEG-phenyls. The signals from sites named only using numbers usually overlap in the aliphatic region, and thus were not treated with any particular interest outside of the peak assignment section.

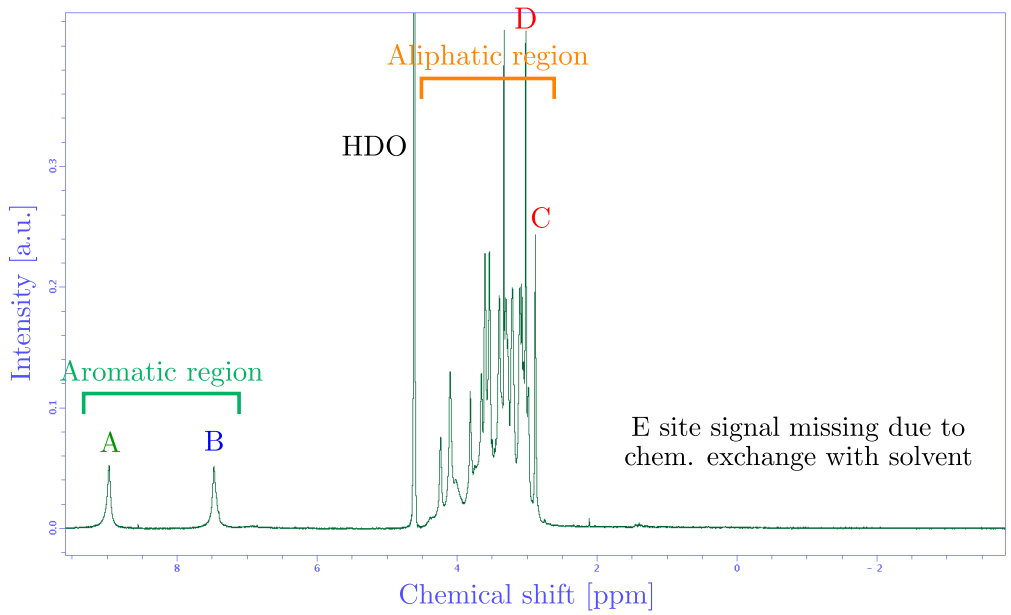

Figure 4.2: ^{1}H spectrum of **3,4,5-TEG-TPP** in D_2O at room temperature. The triplet-like multiplets in aliphatic region are not well resolved. In order to resolve them we measured spectra in $CDCl_3$, for that and **TEG** multiplet assignment see Figure 4.4.

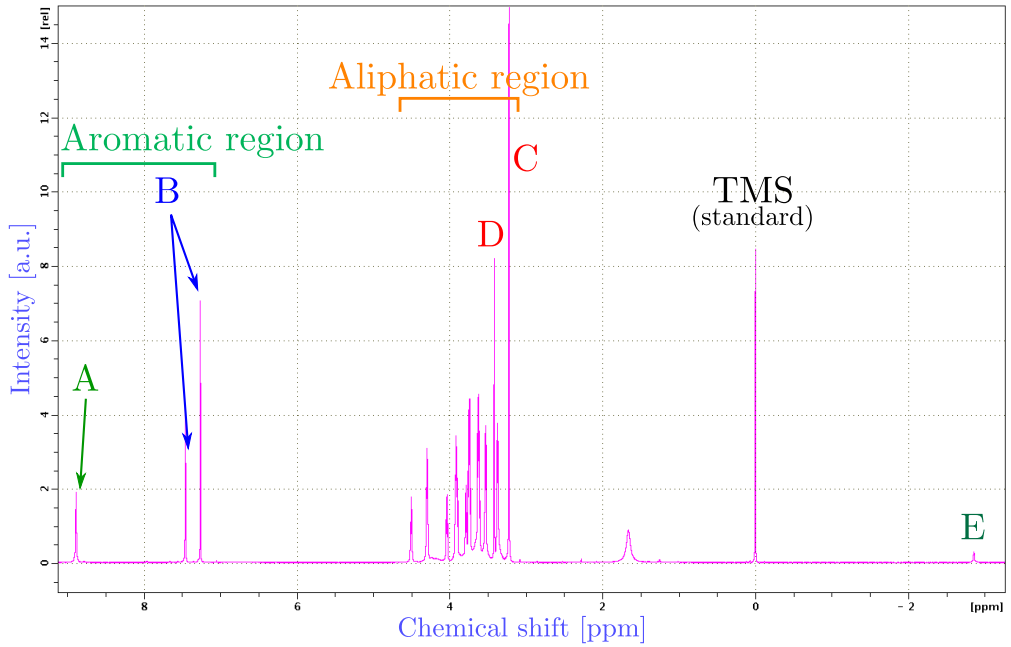

Figure 4.3: ^{1}H spectrum in $CDCl_3$ (chloroform) at room temperature. The peaks of the aromatic region are shifted to large chemical shift values due to the ring current effect. The next Figure 4.4, features enlarged aliphatic region with its detailed assignment. At 0 ppm, the tetramethyl silane (TMS) standard can be seen. The proton peak from NH groups (E sites) can be seen near -3 ppm due to the absence of chemical exchange with solvent; in aqueous solution the peak is nowhere to be found.

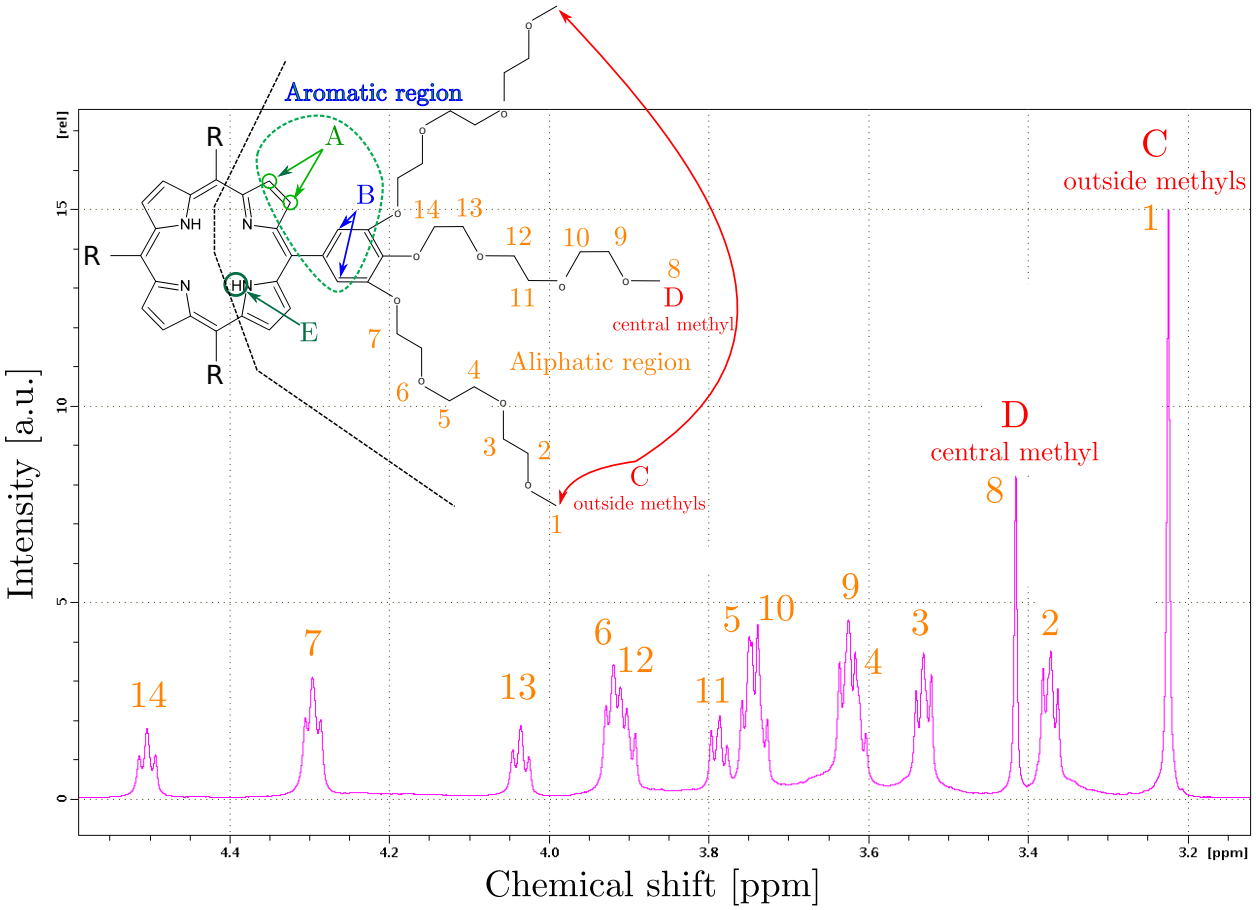

Figure 4.4: Aliphatic triplet-like multiplet region of the ^{1}H spectrum of **3,4,5-TEG-TPP** in $CDCl_3$, peak assignment at room temperature. The reason the peaks are resolved to a much larger degree than in aqueous solution, is the absence of hydrophobic effect in $CDCl_3$. In D_2O, the omnipresent hydrogen bonds cause short-range ordering of water molecules, especially near non-polar solutes [25]. This leads to an increase in time correlation of B_{loc} and consequently in the shortening of T_2, meaning broader peaks. As the distance from conjugated electron systems grows, the ring curent effect gets weaker and weaker, and multiplets shift to lower frequency.

^{13}C peak assignment

The site naming of ^{13}C peaks is shown in the Figure 4.5. In the next figure – the Figure 4.6 – a ^{13}C spectrum in D_2O measured at room temperature is shown. There are two additional views of the spectrum, with gradually increased magnification: the aromatic region with methyl end groups are shown in the Figure 4.7 and merely the aliphatic region with counted peak masses is shown in the Figure 4.8. As will be seen in the Figure 4.9, the ^{1}H and ^{13}C chemical shifts do not correlate monotonously in the aliphatic region.

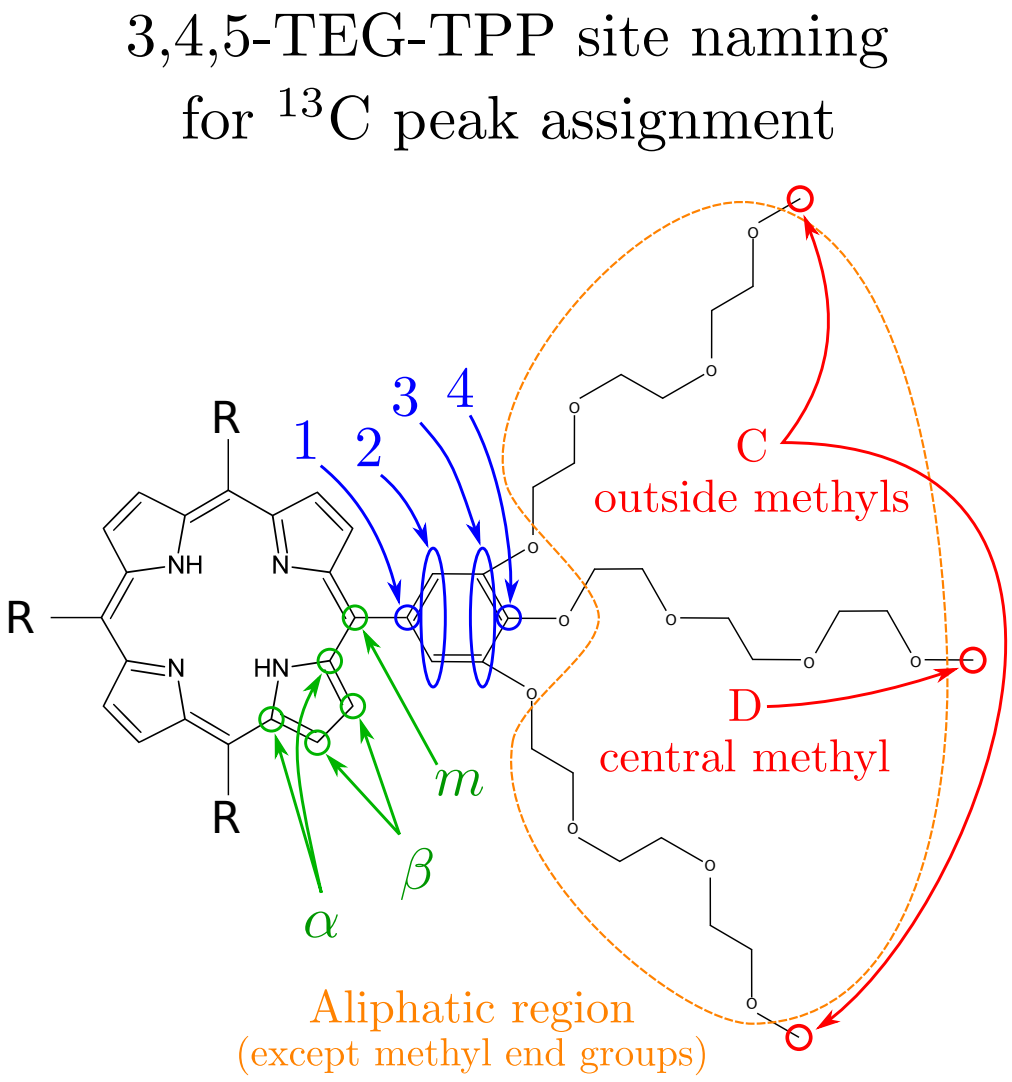

Figure 4.5: Site naming for the ^{13}C peak assignment. The α, β, m sites are named conventionally for porphyrins; the naming is reminiscent of the naming for aminoacids, where the Greek letters start at the first closest carbon to the nitrogen from the amino group; and m is an abbreviation for "meso". The letter "R" stands for the other three 3,4,5-TEG-phenyls. Although the overlapping signals from the aliphatic region were not resolved well, we managed to count them in the Figure 4.8 and arrive at the expected numbers (6 peak pairs, plausibly with 2:1 area ratio in each pair).

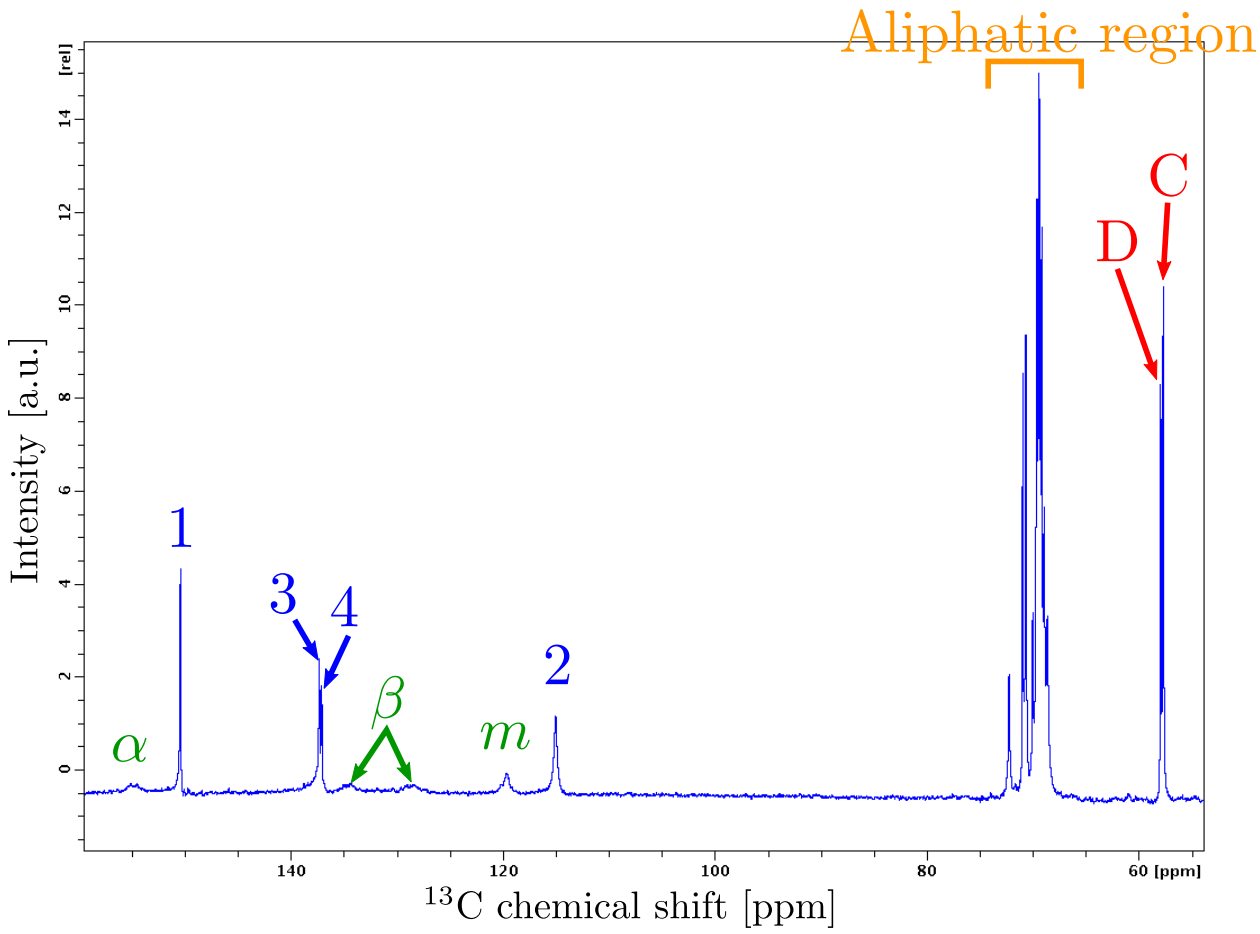

Figure 4.6: ^{13}C spectrum of **3,4,5-TEG-TPP** in D_2O at room temperature, with peak assignment. The 1–4 peaks from phenyls are significantly narrower than the α, β, m peaks from the macrocycle due to the rigidity of the macrocycle and the relative rotational mobility of the phenyls. The phenyl peaks that are the furthest from the macrocycle are also bound to electronegative oxygens, and that is the reason they are shifted to higher chemical shift values (they are deshielded). The β peak seems to be split, which could be due to an assymetry of the porphyrin stacking . The aliphatic region and the D, C end groups are the focus of the next figure, the Figure 4.7.

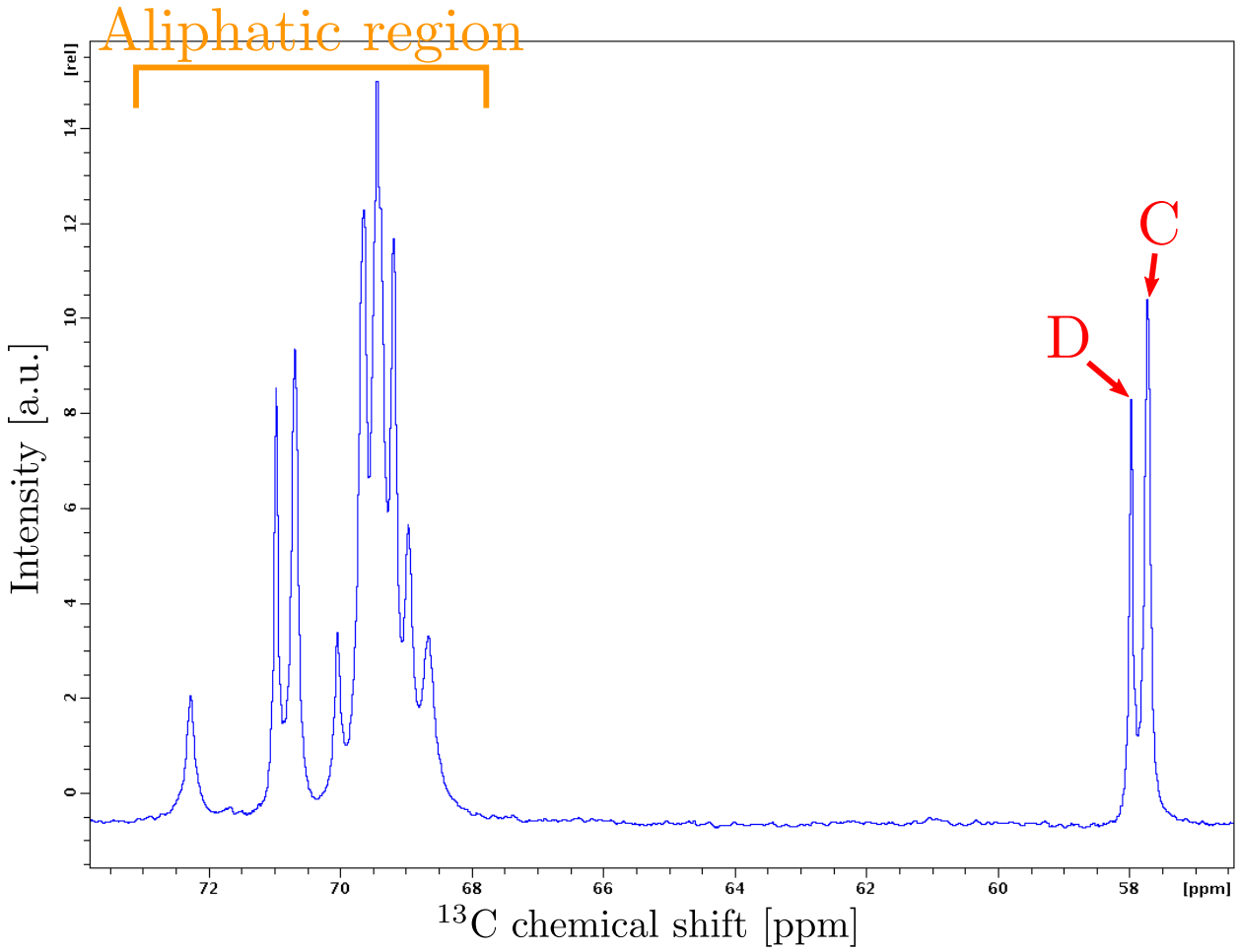

Figure 4.7: The aliphatic region and the methyl end groups part of the ^{13}C spectrum of **3,4,5-TEG-TPP** in D_2O at room temperature. Since decoupling was used during the signal acquisition, the proportionality of peak areas is not a reliable way of comparing signals from sites with different numbers of hydrogens bound to those carbons. However, we only need to compare methyls with methyls and carbons in TEG-like chains with carbons in TEG-like chains. The peak C has double the area of the peak D, as it should. In the next figure, the Figure 4.8 the visible peaks (overlapped multiplets) were counted.

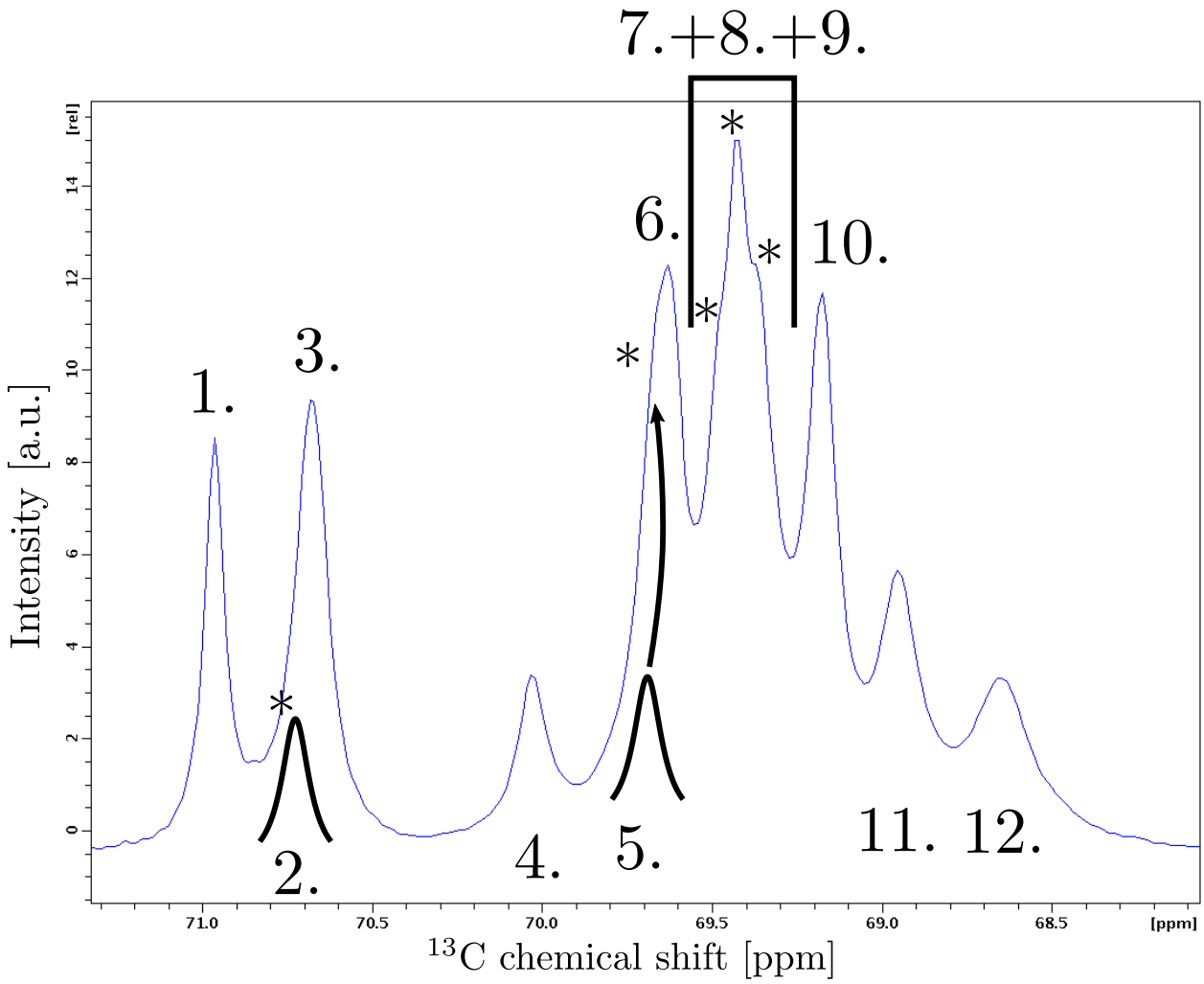

Figure 4.8: The aliphatic region part of the ^{13}C spectrum of **3,4,5-TEG-TPP** in D_2O at room temperature. We have already identified the hydrogen signals in the Figure 4.4. The carbon peaks overlap badly but that is of no consequence, since we still managed to count them. The carbon peaks should follow a similar chemical shift pattern, and should be split into six pairs with the area ratio 2:1 in favor of the outside chains like the hydrogen multiplets were. The asterisks were used to emphasize the sections of the spectrum which seem to imply the existence of some less resolved peaks. Instead of the peak naming from the Figure 4.4 we used ordinal numerals and put the numbers of the obviously smaller peaks at the bottom. The three peaks seventh, eighth and ninth cannot be told apart conclusively and the small one cannot be identified by the naked eye. Fitting could help, but the information is of no use to us and problems with background and likely even non-standard peak shape would have to be solved in the process.

2D heteronuclear correlations

In NMR, there exist many more advanced pulse sequencses that we have not described in the theory part, due to the vast scope of theory that would be required to explain them. To prove that the assignment we performed in the previous figures is correct, we used the Heteronuclear Single Quantum Coherence (HSQC) and Heteronuclear Multiple Bond Correlation (HMBC) experiments. Their pulse sequences involve excitation of one isotope, transfer of magnetization onto its neighbors and subsequent observation of those neighbors. The resulting spectra of both have one axis with ^{1}H chemical shifts and one axis with ^{13}C chemical shifts. The signals that we observe tell us which nuclei interact with which neighbors. HSQC provides us with signals between directly bound nuclei and HMBC excludes the nearest neighbors, but still requires the magnetization to be transferred over bonds, so the sensitivity range expressed in terms of bonds is from 2 up to about 3 or 4.

The Figures 4.9 and 4.10 show the HSQC and HMBC 2D spectra for ^{1}H and ^{13}C of **3,4,5-TEG-TPP**. All the information contained is consistent with the previous assignment, only the order of aliphatic region peaks is not very obvious.

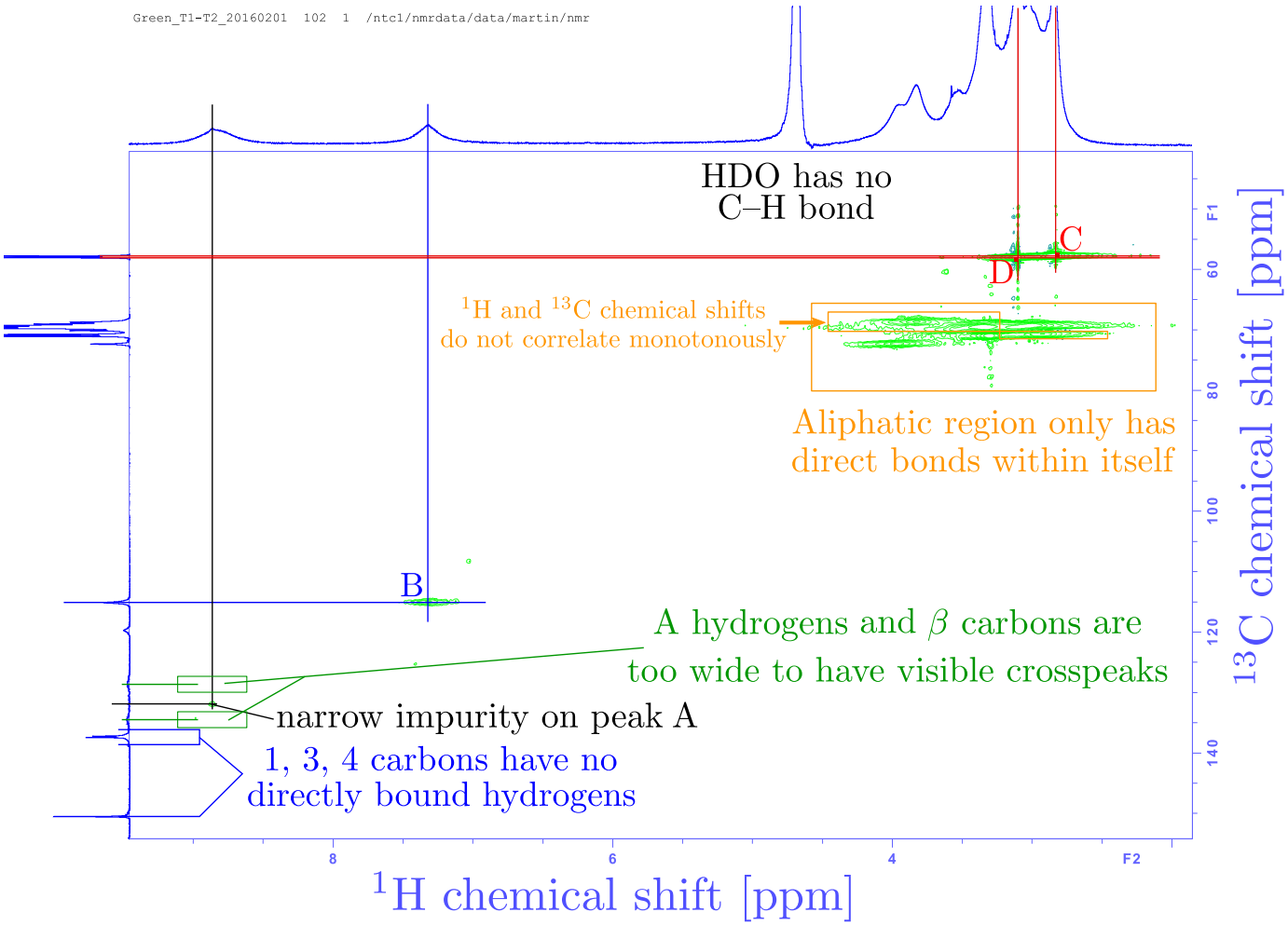

Figure 4.9: ^{1}H–^{13}C HSQC 2D spectrum for in an aqueous **3,4,5-TEG-TPP** solution. All the information supports the assertions from the peak assignment.

HMBC: ^{1}H and ^{13}C that are 2 or 3 bonds apart

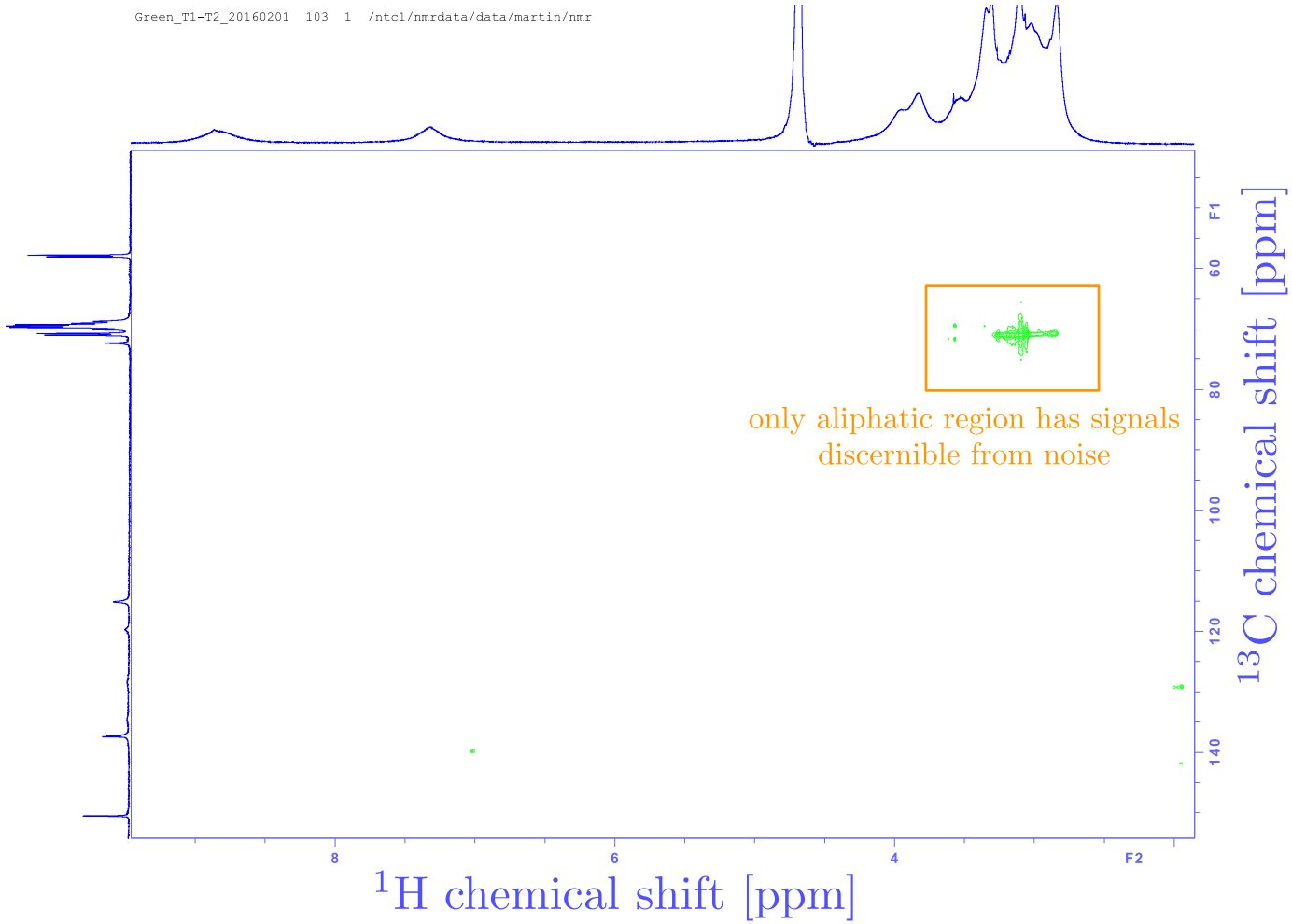

Figure 4.10: ^{1}H–^{13}C HMBC 2D spectrum of an aqueous **3,4,5-TEG-TPP** solution. Due to short experimental time, only the aliphatic signal is discernible from noise. The aliphatic region contains more ^{1}H–^{13}C pairs visible in HMBC than the tetrapyrrolic macrocycle.

4.2 Phase separation and phase diagram

To quantify the phase separation, we measured a VT series for each of the ϕ_P in the Table 4.1. We prepared two samples, and for both we used the dilution and partial removal approach with composition being a geometric series as noted in the Subsection 2.1.1. This way, two volume fraction series were created. The reason we created two of these series was that because the first time around the highest concentration sample was not larger than ϕ_{crit}, we had poor data to fit the binodal to (no minimum). So then we went on creating an approximately $\phi_P = 0.1$ sample and that was finally enough. The volume fractions, molar enthalpy and entropy differences from fitting and the temperatures calculated from these quantities are shown in the table below. The lines with the blue volume fractions belong to the first, lower concentration series, the red ones to the more concentrated series. The green column shows the important T_{ONSET} quantity. The colored columns are the (ϕ_P, T_{ONSET}) datapoints we then fitted the binodal onto. The result of this fitting and also the spinodal corresponding to the binodal are shown in the Figure 4.13.

Table 4.1: Measured VT datasets overview

$\phi_P[\%]$	$\Delta h[kJ/mol]$	$\Delta s[kJ/mol/K]$	$T^{crit}[K]$	$T_{ONSET}[K]$	$T_{ONSET}[°C]$
9.334	11672	36.60	319.0	318.8	45.66
8.109	8360	26.26	318.6	318.2	45.01
6.850	2903	9.082	319.6	319.0	45.88
5.437	2113	6.616	319.4	318.6	45.41
4.127	2346	7.341	319.6	318.9	45.70
3.001	1149	3.581	320.8	319.3	46.12
2.348	631.6	1.957	322.7	320.0	46.83
1.834	762.7	2.367	322.2	319.9	46.77
1.188	465.5	1.432	325.2	321.4	48.27
0.597	469.5	1.431	328.0	324.2	51.06
$267.8.10^{-3}$	390.8	1.180	331.1	326.5	53.32
$179.4.10^{-3}$	344.5	1.027	335.4	330.0	56.84
$67.37.10^{-3}$	310.3	0.9178	338.1	332.0	58.84
$33.69.10^{-3}$	325.8	0.9570	340.5	334.6	61.44
$16.86.10^{-3}$	277.5	0.8025	345.8	338.7	65.51
$8.420.10^{-3}$	285.6	0.8210	347.9	340.9	67.72

The majority of the processing procedures is schematically shown in the Figure 4.12, and as a whole it can be summarized as:

1. Each of the points in – for example the Figure 4.11 – was acquired by fitting each spectrum of that particular series with Lorentzian, or for large ϕ_P pseudo-Voigt curves into peaks corresponding to the aromatic region A, B (and their phase-separated counterparts A', B' when necessary) and C' from the aliphatic region, as described in the Section 3.2.

2. After fitting all the spectra with peaks, all of the $f_{sep}(T, \phi_P)$ points become available. For each of the VT series (i.e. fixed ϕ_P) we find one $f_{sep}(T)$ curve given by the Equation 3.4 and acquire a $(\Delta h, \Delta s)$ pair. The results are in the Table 4.1.

3. We use these $(\Delta h, \Delta s)$ pairs to calculate the (ϕ_P, T_{ONSET}) points on the binodal, as described in the Section 3.3. We fit a binodal curve onto those points as described in the section 3.4. The experimental (ϕ_P, T_{ONSET}), resulting binodal, spinodal and the tuple (r, A, B) of this fit are all shown in the Figure 4.13

The resulting value of r after binodal fitting is 309.38. The molar mass of the **3,4,5-TEG-TPP** molecules is 2560 g/mol, the value of molar mass of D_2O is approximately 20 g/mol. By comparing the obtained value

of r with the ratio of molar masses of **3,4,5-TEG-TPP** and D_2O which is approximately 128, we conclude that the porphyrin forms dimers under LCST in aqueous solution.

The density of **3,4,5-TEG-TPP** used in our calculations of the volume fractions ϕ_P was determined by our colleagues at NIMS; the value is 1.595 g/cm^3.

When performing the experiments, the composition parameter most accessible to us is the *weight fraction* denoted w_P and defined in the Equation 4.1 below. Our desired composition parameter is the porphyrin volume fraction ϕ_P, however. Its definition is the Equation 4.2. In order to calculate the ϕ_P, the Equation 4.4 was used. The inverse is the Equation 4.5. For the calculation of molar concentration, Equation 4.6 was used.

$$w_P = \frac{m_P}{m_P + m_{D2O}} \tag{4.1}$$

$$\phi_P = \frac{V_P}{V_P + V_{D2O}} \tag{4.2}$$

$$m_P = \rho_P V_P \tag{4.3}$$

$$\phi_P = \frac{1}{1 + \frac{\rho_P}{\rho_{D2O}} \left(\frac{1}{w_P} - 1 \right)} \tag{4.4}$$

$$w_P = \frac{\rho_P \phi_P}{\rho_{D2O} + (\rho_P - \rho_{D2O})\, \phi_P} \tag{4.5}$$

$$c_P = \frac{\rho_P}{M_P} w_P \tag{4.6}$$

The higher the volume fraction of the porphyrin, the shorter the slope of the function $f_{sep}(T)$. This is demonstrated in the Figure 4.14. This is because the molar Δh and Δs values acquired by NMR do not necessarily correspond to moles of molecules; instead they correspond to moles of some clusters. For example in polymers they correspond to moles of some cooperating units. This can be seen in the Table 4.1 as the values of both Δh and Δs being strongly dependent on ϕ_P; but the ratio of Δh and Δs is T^{crit} – a very tame quantity.

One phenomenon we did not explain yet is the A and B splitting into two new peaks at high temperatures, which can be seen in the Figure 4.15. This happened for the samples with the volume fraction ϕ_P closest to the ϕ_P^{crit}.

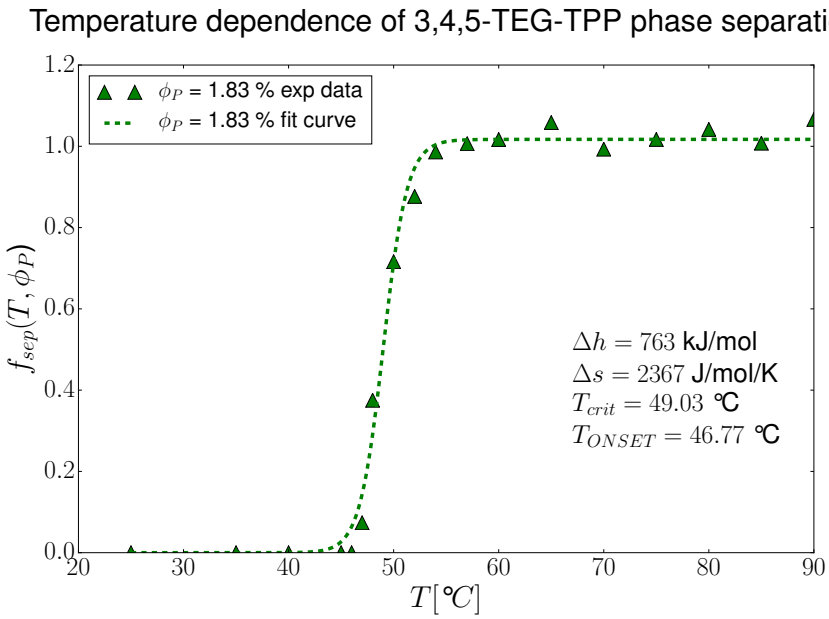

Figure 4.11: $f_{sep}(T)$ fit example. After processing all of the 1D spectra into $f_{sep}(T, \phi_P)$ points we fitted the $f_{sep}(T)$ dependence for each of the fixed ϕ_P values. The fit curve is the theoretical form of f_{sep} given by the Equation 3.4. The direct result of such a fit is one $(\Delta h, \Delta s)$ pair. All of the acquired pairs are shown in the Table 4.1. For each such pair, T_{ONSET} was then calculated as shown in the same table, the Table 4.1, using the green text coloring. This was done by the procedure explained in the Section 3.3. This fitting was done and the plots were created by running a script I created in the Python programming langue (its *Anaconda* distribution [26]).

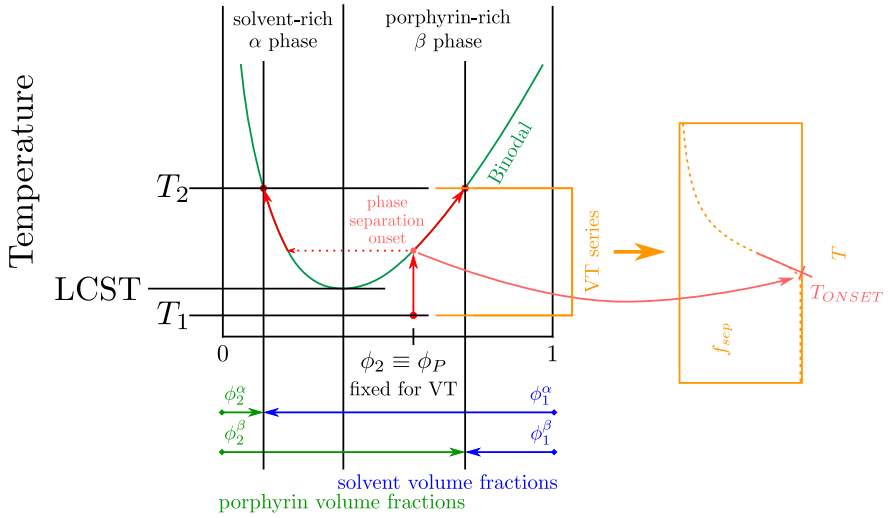

Figure 4.12: Illustration of the important objects and procedures used in the quantification of phase separation. We prepare a sample at a point of perfect miscibility (ϕ_P, T_1), e.g. $(3\%, 25°$ C). The sample is then gradually heated up to some temperature, for example 90°C. 1D spectra are measured throughout. At some T_{ONSET} the solution begins to separate into two phases, α and β. This is quantified by fitting the spectra afterwards. From one such series, one T_{ONSET} is obtained. The meaning of $\phi_1^\alpha, \phi_2^\alpha, \phi_1^\beta, \phi_2^\beta$ is depicted at the bottom of the figure.

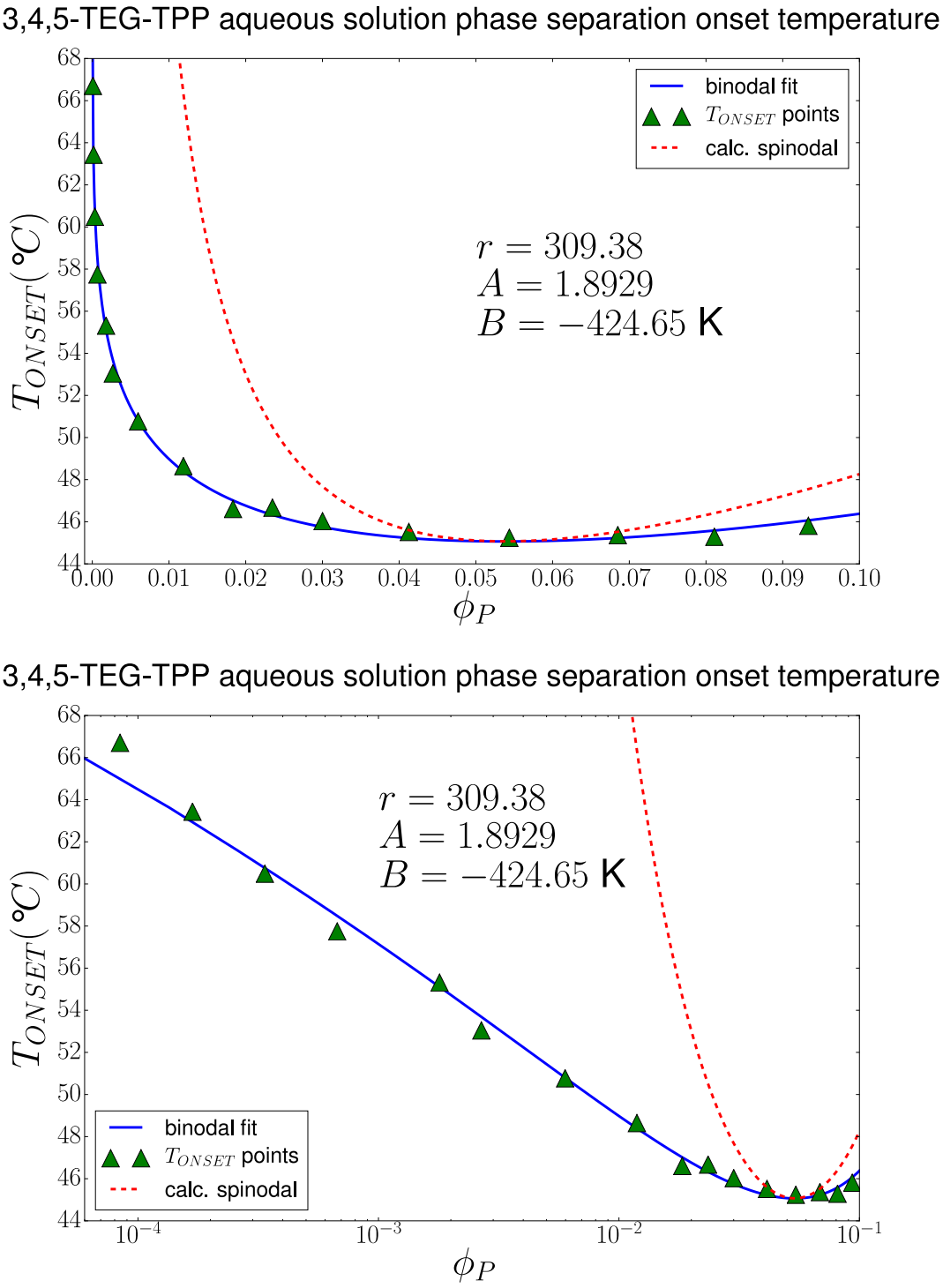

Figure 4.13: The main result of this thesis, the *temperature-composition phase diagram of the aqueous solution of* **3,4,5-TEG-TPP**. The ratio of molar masses of the compound and heavy water being approximately 128, the interpretation of $r \approx 310$ according to the Liquid Lattice Theory suggests that **3,4,5-TEG-TPP** forms dimers (with some effective solvation layer presumably). Using the Equations 3.11 and 3.12 the values of (r, A, B) can be used to calculate $LCST = 45.0°\text{C}$, at $\phi_P^{crit} = 5.378\%$. The formation of larger stacks is likely prevented by the entropic penalty due to the **TEG**-like chains acting as sterical barriers and thus reducing the number of self-avoiding microstates of a tri-plus-mer significantly.

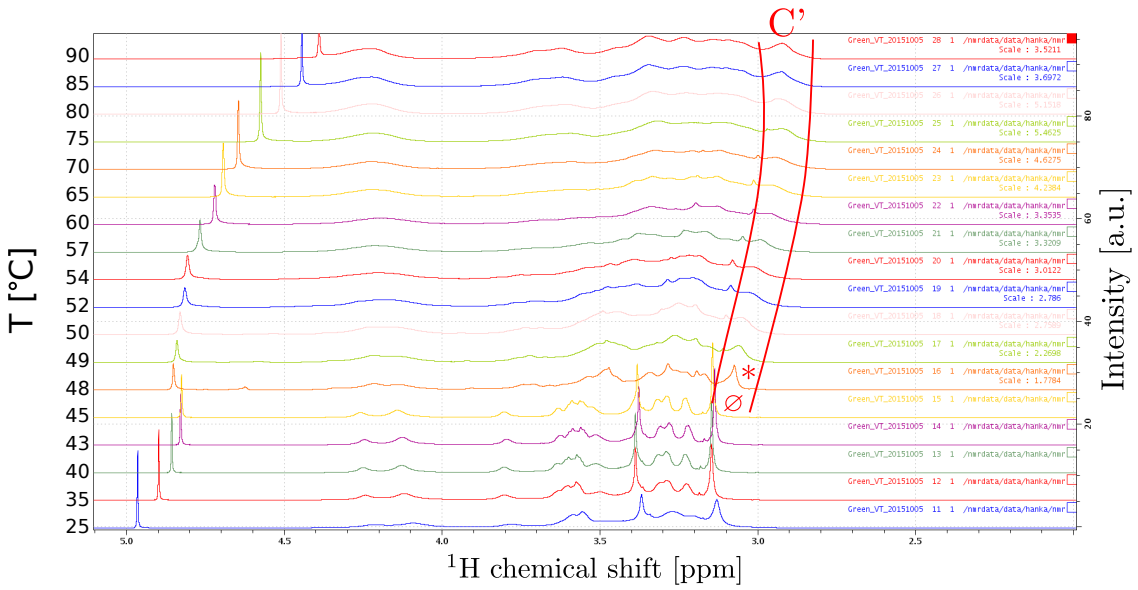

Figure 4.14: The VT series with the highest volume fraction of the **3,4,5-TEG-TPP** porphyrin. The C' peak of the phase-separated **3,4,5-TEG-TPP** side methyl end groups that we use to measure the phase separation appears very suddenly (temperature 45–48°C).

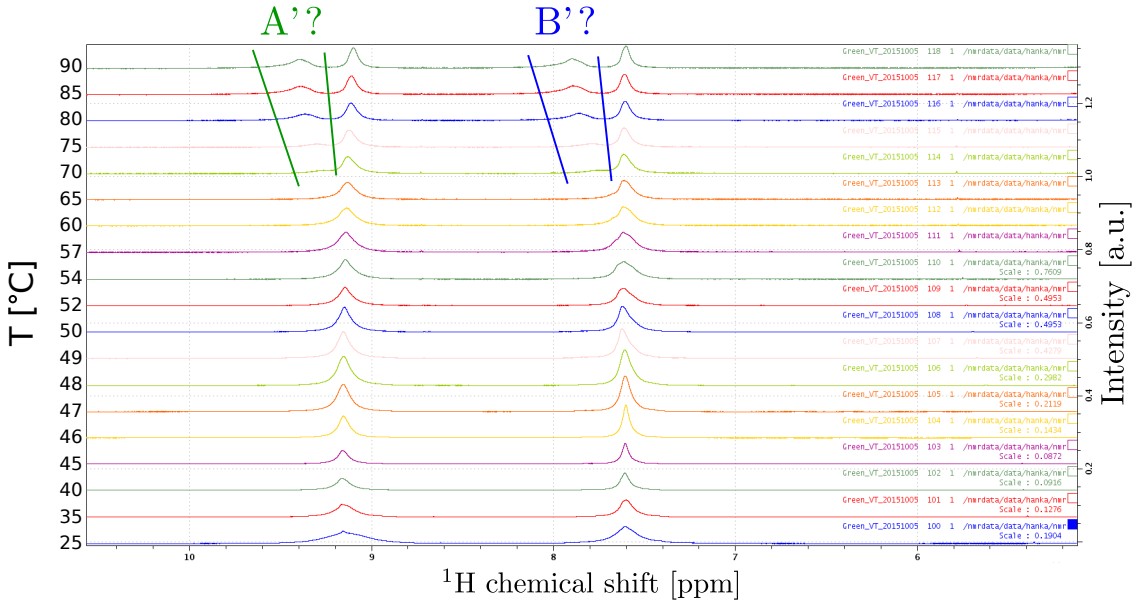

Figure 4.15: A VT series of 1D ^{1}H spectrum of **3,4,5-TEG-TPP** with $\phi_P = 6.85\%$; there is no acid in the solution. We have no satisfactory explanation as to why the peaks to the left appear, yet. Although this also happened for the next sample (with $\phi_P = 5.437\%$), the A' and B' peaks for other samples were always overlapping with A and B. The **3,4,5-TEG-TPP** molecules obviously adopt some new form with very slow chemical exchange, but we did not find out what it is.

4.3 Host-guest interactions with acid

The interaction between **3,4,5-TEG-TPP** molecules and the solvent has been sufficiently characterized. The porphyrins are known to bind positive ions and form complexes. This behavior could also in principle affect the phase separation that we studied. We went on and performed titrations of the **3,4,5-TEG-TPP** solution with *S*-camphorsulfonic acid, shown in the Figure 4.16.

After adding the acid into the solution, splitting and narrowing of peaks occured. This is shown in the Figures 4.17 and 4.18 Our interpretation of the peak splitting and narrowing is shown in the Figure 4.19.

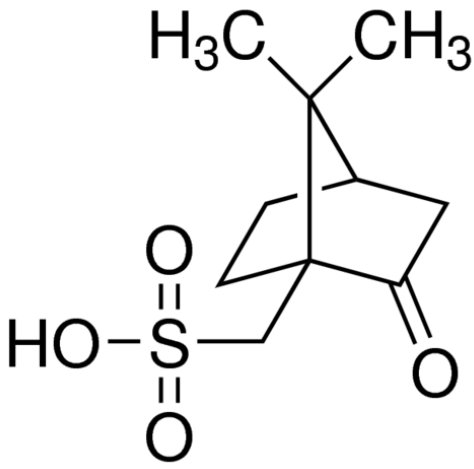

Figure 4.16: *S*-camphorsulfonic acid. We used this compound in titrations of **3,4,5-TEG-TPP** solutions to investigate the host-guest interactions of **3,4,5-TEG-TPP** with positive ions and/or the acid as a whole. The image was taken from the *Sigma-Aldrich* website [27].

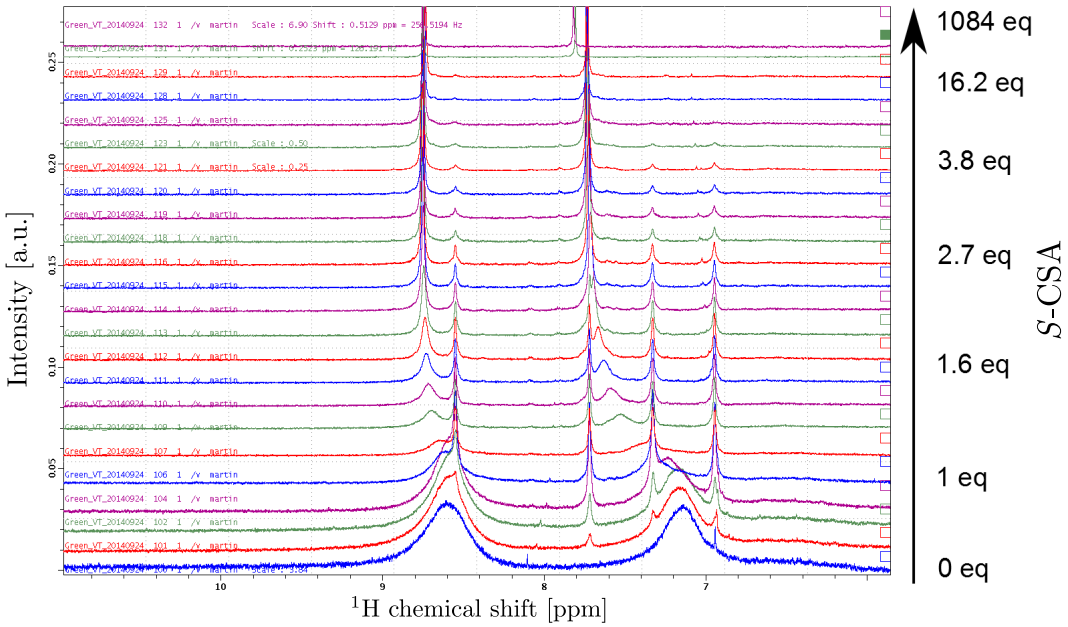

Figure 4.17: The aromatic part of the ^{1}H spectrum of the aqueous solution of **3,4,5-TEG-TPP** with various amounts of *S*-camphorsulfonic acid. One equivalent of acid means there was one molecule of **S-CSA** per one molecule of **3,4,5-TEG-TPP** in the solution.

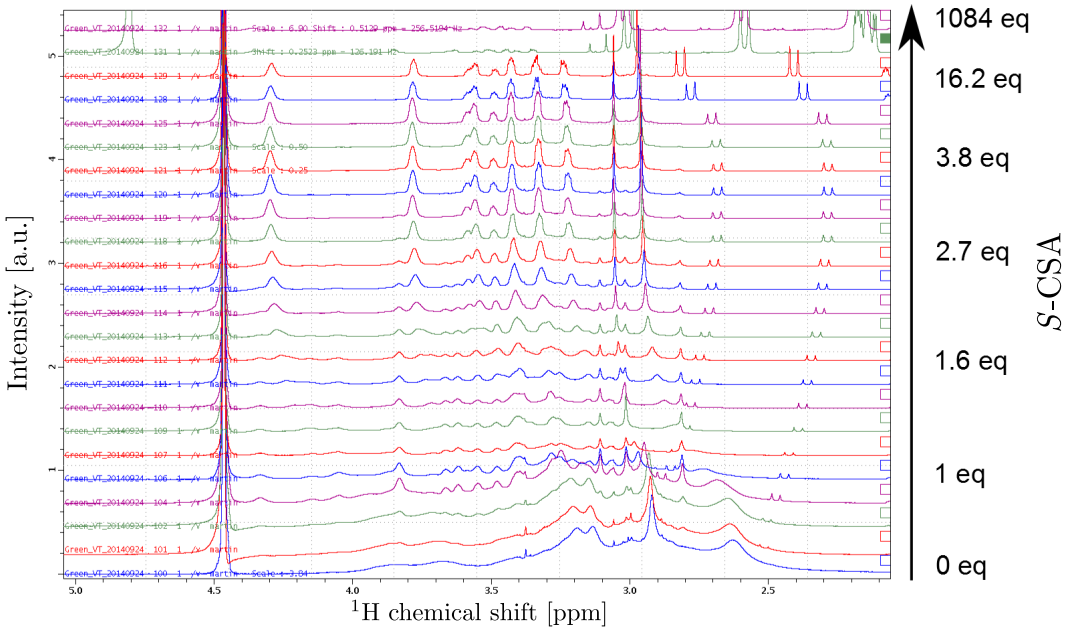

Figure 4.18: The aliphatic part of the ^{1}H spectrum of the aqueous solution of **3,4,5-TEG-TPP** with various amounts of *S*-camphorsulfonic acid. At low *S*-CSA content, the peaks are relatively broad, which is consistent with our findings about the porphyrin stacking. From this stack plot we can clearly see that somewhere between 2 *eq* to 2.7 *eq* of acid the porphyrin molecules all start to take on the same state, since all of the peaks become well-defined and narrow. We interpret this as the un-stacking of porphyrin molecules; the protonation of **3,4,5-TEG-TPP** molecules charges the center of the macrocycle positively which causes the molecules to spread apart.

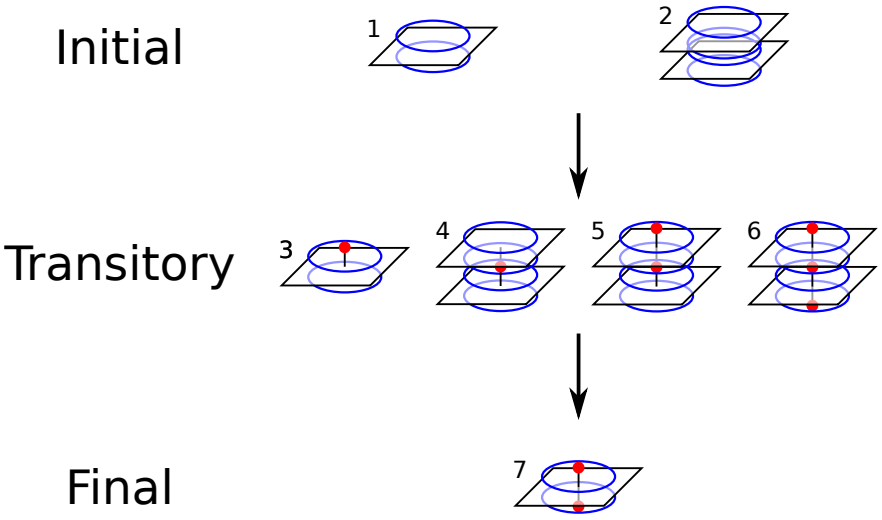

Figure 4.19: Our interpretation of the data in the two previous figures, the Figures 4.17 and 4.18. We know that **3,4,5-TEG-TPP** forms predominantly dimers. Once acid is added, those start to break down in proportion to the amount of acid. The splitting of the aromatic region peaks shows that several transitory protonated forms coexist. From the peak widths and phase separation results we can say that no larger **3,4,5-TEG-TPP** stacks than protonated dimers can exist. From the stoichiometry of protonation (from 2–2.7 eq the signals become identical) we conclude that the most populated final form of **3,4,5-TEG-TPP** is the doubly protonated form 7 at the bottom.

We also investigated how the *S*-CSA content affects the phase separation. We measured VT series for samples with various amounts of *S*-CSA added and the resulting $f_{sep}(T)$ acquired by fitting the spectra are shown in the Figure 4.23. With increasing *S*-CSA content the phase separation is shifted to higher temperatures and its extent is lowered. The Figures 4.20 to 4.22 contain the VT series stack plots of **3,4,5-TEG-TPP** solutions with three different amounts of added acid: 0 eq, 3 eq and 20 eq. At 20 equivalents (the Figure 4.22) the C' peak can be barely seen even at an extreme magnification of the spectrum.

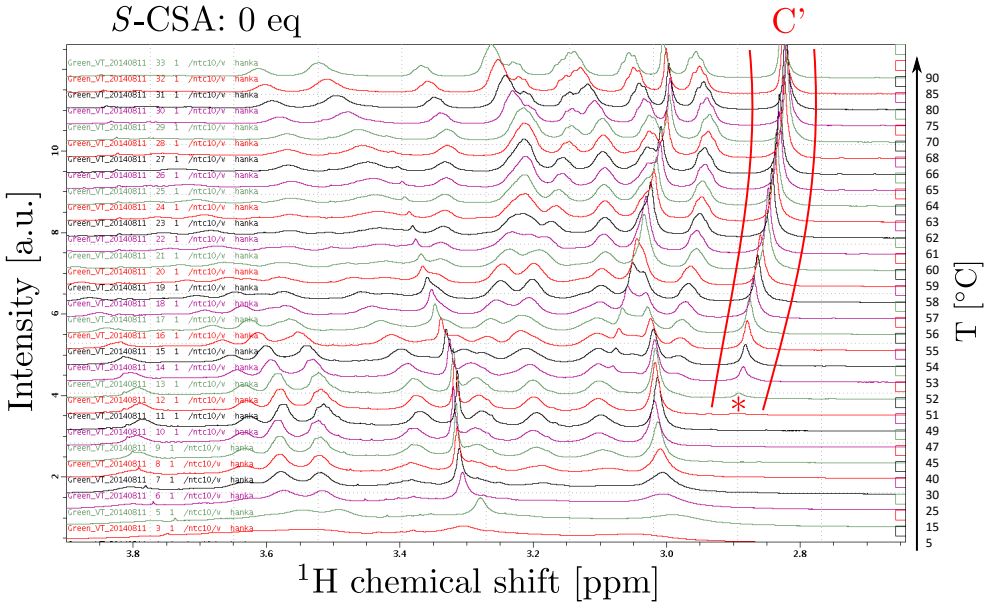

Figure 4.20: A VT series of an aqueous **3,4,5-TEG-TPP** solution with no *S*-CSA. The phase separation starts at about 51°C. Compare this stack plot with the following figures, the Figures 4.21 and 4.22.

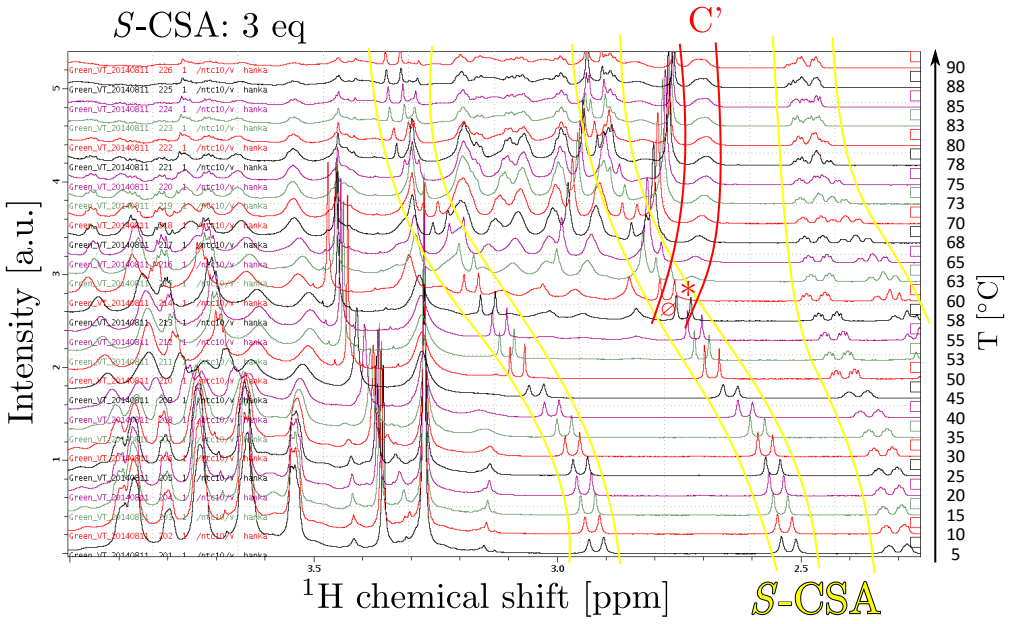

Figure 4.21: After adding 3 eq of *S*-CSA the temperature of phase separation shifted to about 60°C. The *S*-CSA peaks are between the yellow curves.

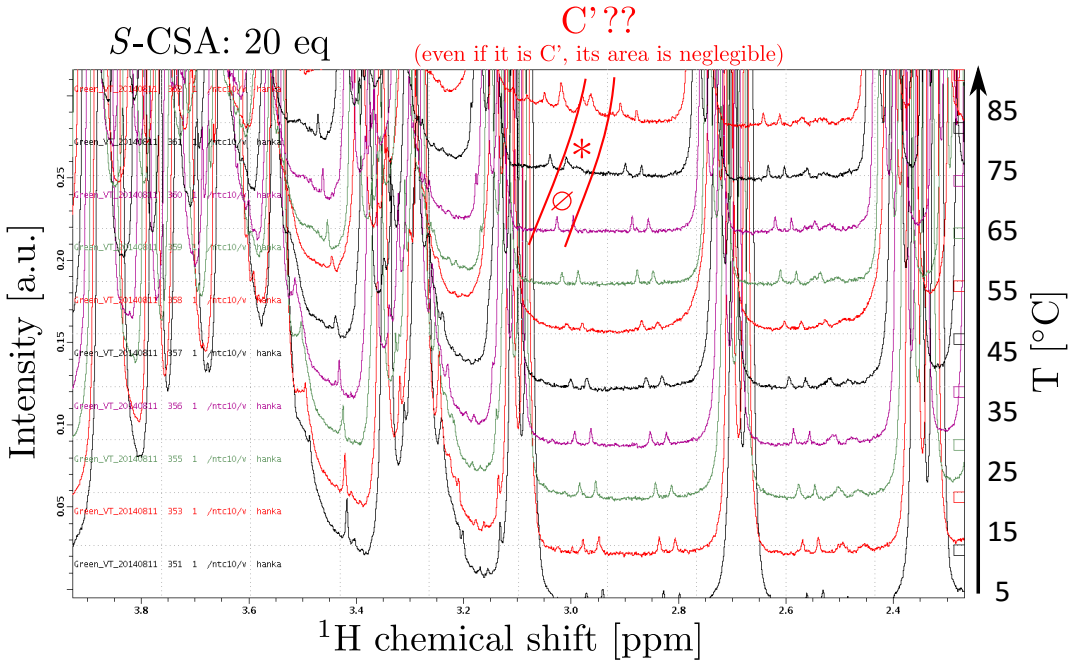

Figure 4.22: The stack plot of a VT series of an aqueous **3,4,5-TEG-TPP** solution with 20 equivalents of *S*-CSA, with very large magnification. The phase separation starts at nearly 75°C. Due to the very small amount of phase-separated porphyrin, the phase separation occurs to a very small extent.

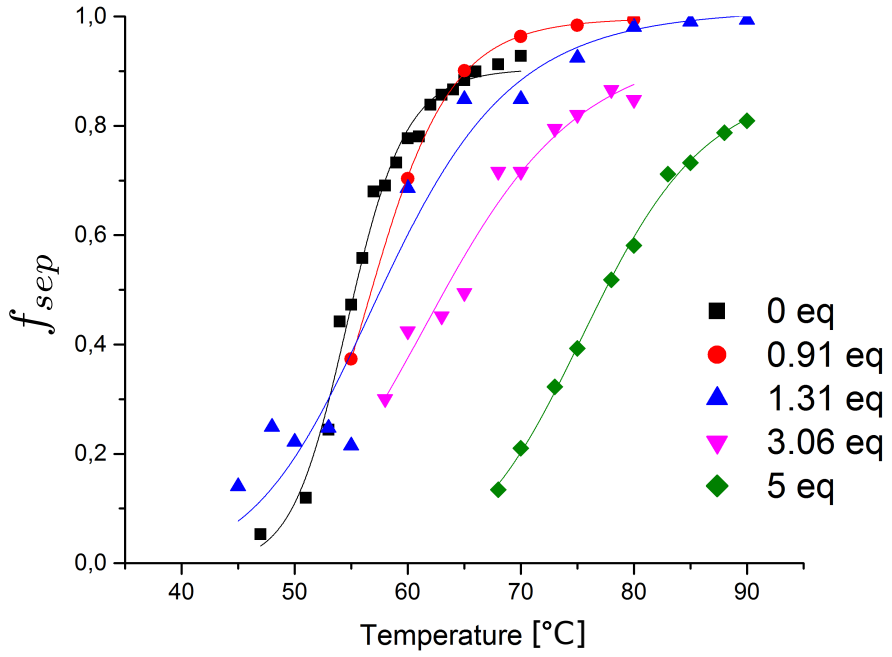

Figure 4.23: By the addition of *S*-CSA, phase separation is shifted to higher temperatures and its extent is lowered. Each point was acquired by fitting the spectra the same way we fitted the phase diagram data.

4.4 VT of 3,4,5-TEG-TPP in $CDCl_3$

We also measured a VT series in $CDCl_3$. The experiments showed that in chloroform, there is an additional process to be found: at the temperature range of about -40 to -10°C the chemical exchange of hydrogens on the NH and N groups slows down, which causes splitting of the A peaks. The result is shown in the figure below:

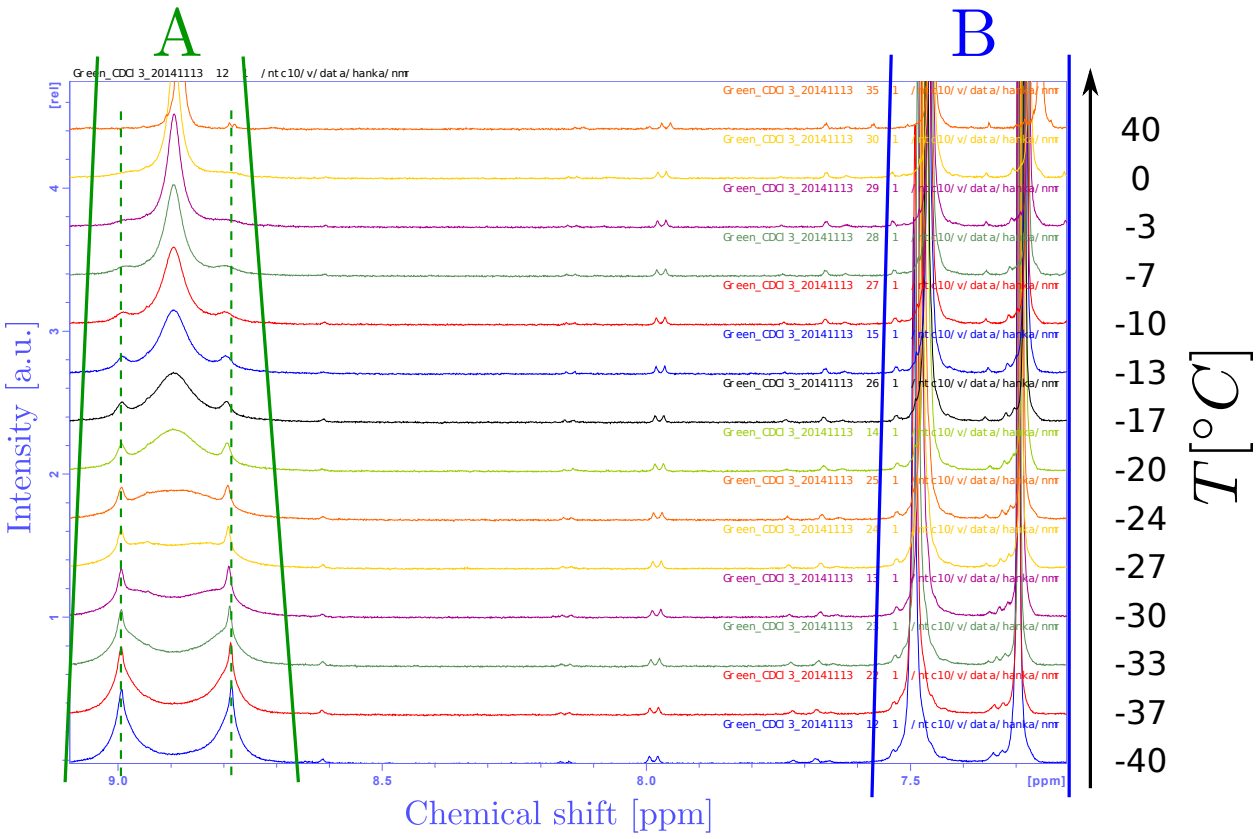

Figure 4.24: A stack plot of a VT series of a $CDCl_3$ **3,4,5-TEG-TPP** solution. The peak splitting implies the slowing down of the chemical exchange of H on the central N and NH groups; which is very slow at temperatures about -40° and increases its mean frequency as the temperature becomes positive. The very narrow peaks at various chemical shifts are impurities.

4.5 Optical microscopy

My colleagues, my supervisor RNDr. Hana Kouřilová, Ph.D and her undergraduate student Monika Spasovová also work on some experiments using the optical microscope. Their aim is to determine the β-phase droplet size distribution; for both the aqueous **3,4,5-TEG-TPP** solutions with and without acid, at various values of the volume fraction ϕ_P. I included a few micrographs below.

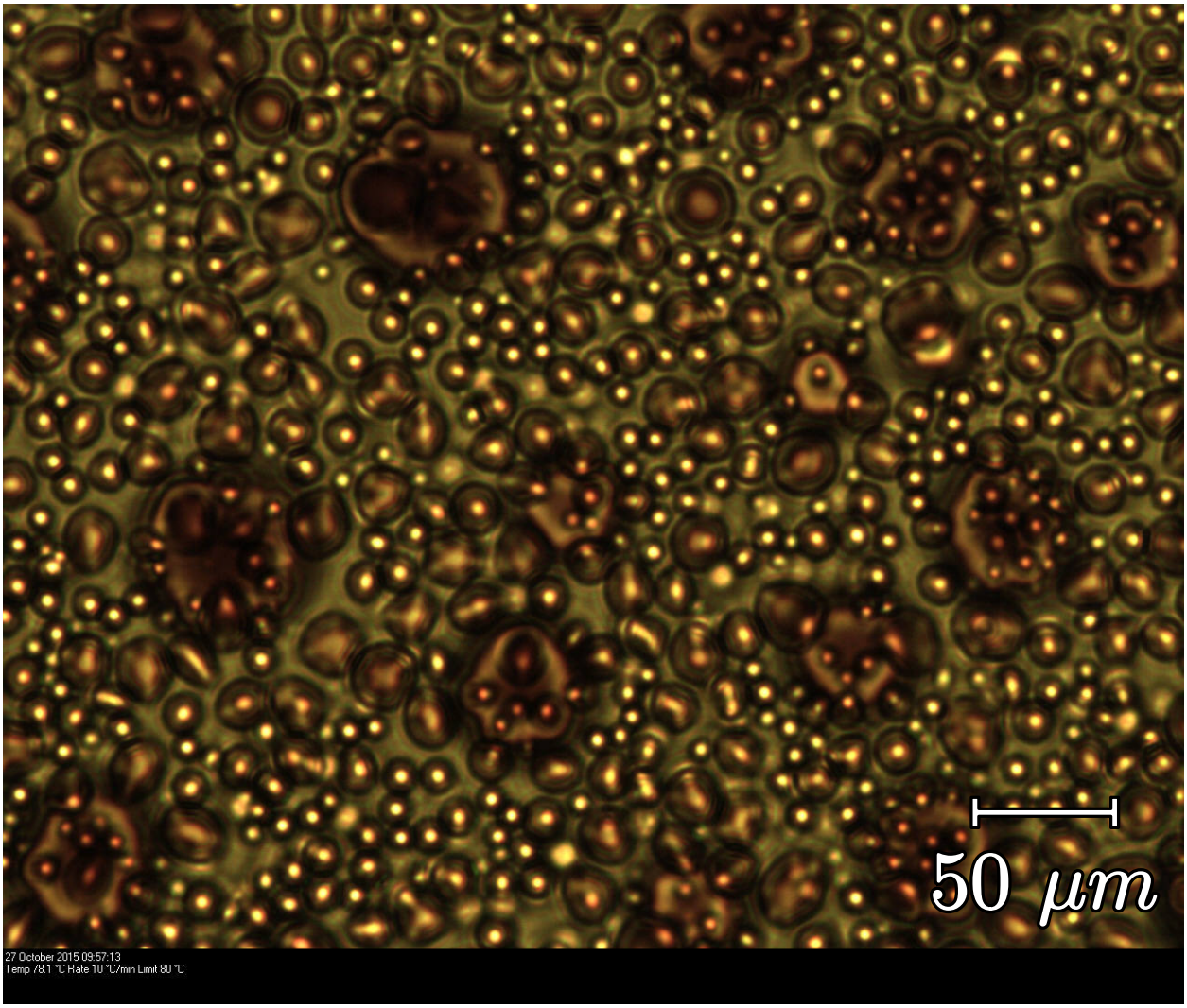

Figure 4.25: A micrograph of a 48 mM **3,4,5-TEG-TPP** water solution, with 0.9 eq of *S*-CSA added during sample preparation. The sample was being heated up, the current temperature was 78.1°C. Obvious concentration gradients exist and the phases are not well-defined yet; the sample is not in equilibrium yet. The solvent-rich phase that is also acid-rich is green, because protonated **3,4,5-TEG-TPP** molecules adopt a saddle-like conformation – which changes the energy levels of the conjugated electron system and causes a significant shift of the molecules' absorbance. The porphyrin-rich phase contains a large portion of molecules which are not protonated and remain red. Some light passes through both the reddish droplets *and* the green solution and in total, much of it is absorbed.

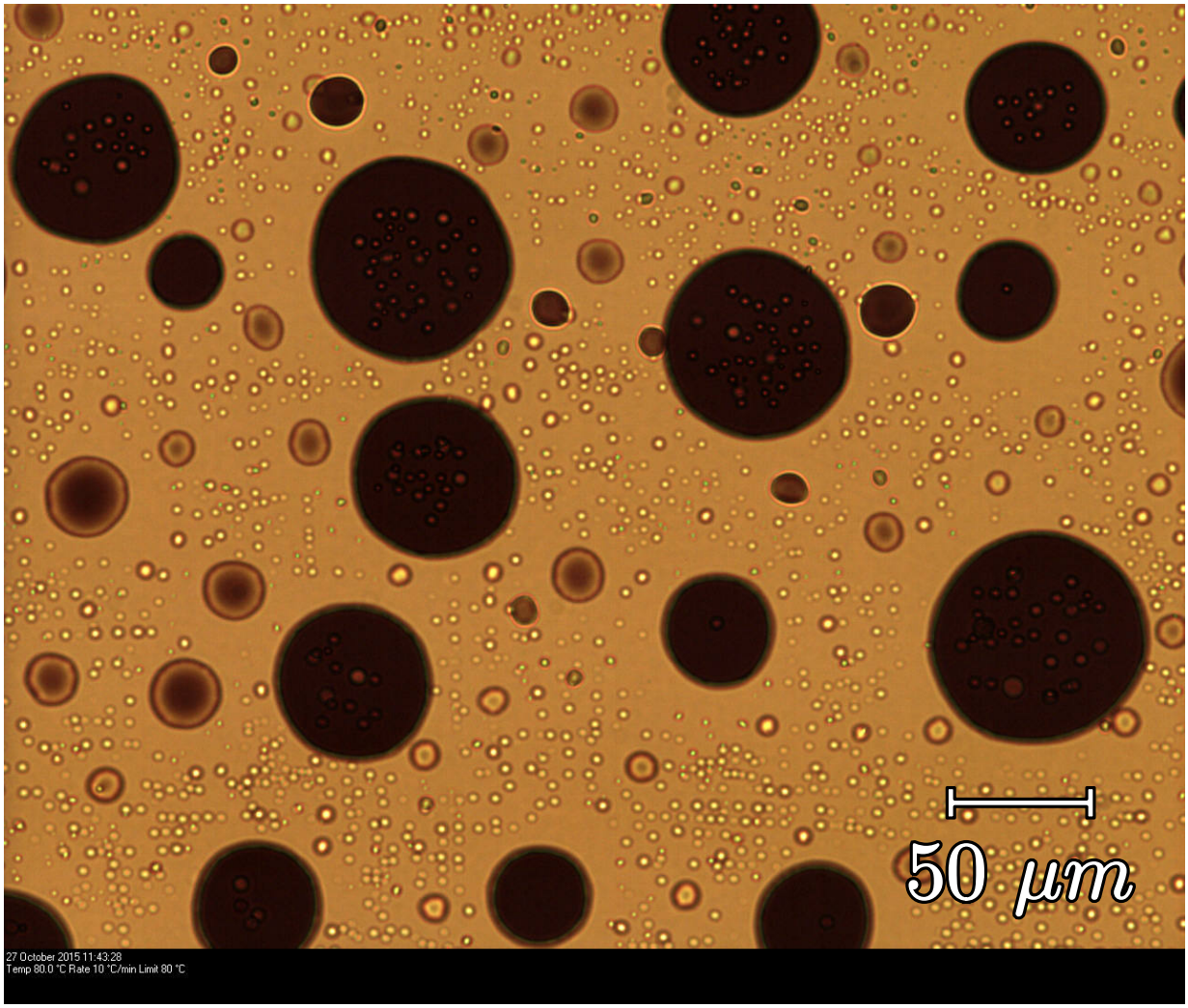

Figure 4.26: The same solution as was shown in the previous figure, about a hundred minutes later. The phase-separated porphyrin forms droplets. It is apparent that in order to minimize the Gibbs energy of the solution, the porphyrin and water only mix in two, well-defined ratios – the solvent-rich α phase and the porphyrin-rich β phase. As the phase sepration continues, the equilibrium porphyrin volume fraction in the oldest and largest droplets shifts to higher values than it was during their creation, while the total composition of droplets only changes slowly (they "sweat" through their surface). A local surplus of water is created and small droplets of the α phase appear within the large β phase droplets. Similarly, a large amount of very small β droplets is created in the α phase. On the whole, the solution looks much lighter than in the previous figure. This is because the porphyrin is mostly concentrated in the droplets and the average porphyrin molecule is in the shadow of its neighbors. The only green part of the solution is the surface of the smallest β phase droplets, where both *S*-CSA and porphyrin exist. Energetically, the porphyrin molecules would prefer to be protonated, but the H^+ cations are electrostatically attracted to the hydrophilic *S*-CSA in the α phase. As a result, the solution is slightly red and slightly green, being somewhat yellow/brown on the whole.

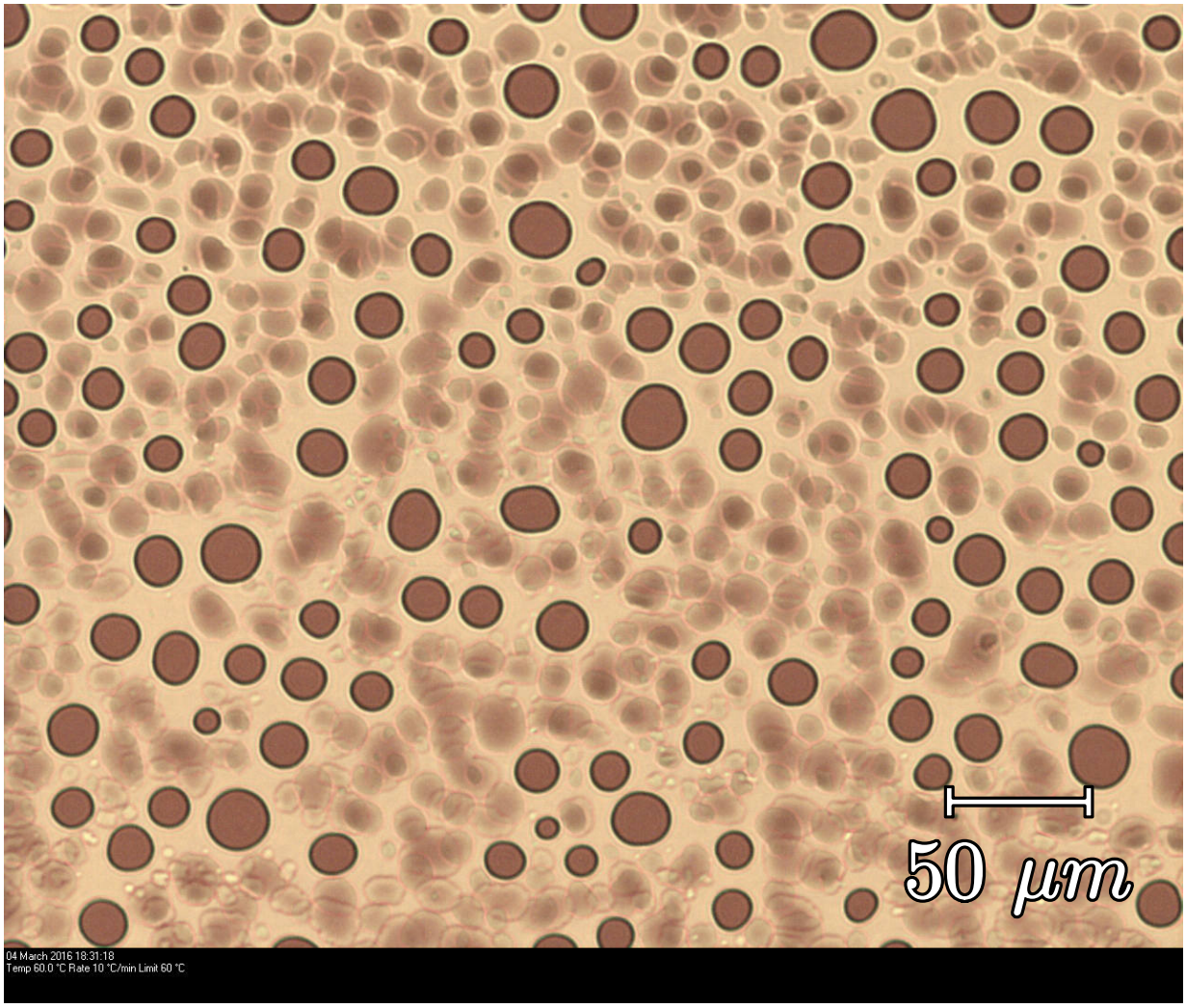

Figure 4.27: Aqueous solution of **3,4,5-TEG-TPP** with no acid. This polarized light micrograph shows no existence of nematic phase. Loci with liquid-crystal-like short-range order would show up as clearly identifiable Schlieren textures; as it stands, we only see the amorphous, porphyrin-rich β phase droplets immersed in the dominant solvent-rich α phase.

Conclusions

By performing NMR experiments and application of the Flory-Huggins Liquid Lattice Theory of Polymer Solutions we learned that **3,4,5-TEG-TPP**:

- undergoes phase separation when heated up and we obtained the phase diagram of this process. According to the Flory-Huggins theory the binodal, spinodal, LCST and ϕ_P^{crit} are uniquely given by the parameter tuple $(r, A, B) = (309.38, 1.8929, -424.65K)$. The binodal and spinodal are shown in the Figure 4.13; we calculated the coordinates of the binodal minimum: $(\phi_P^{crit}, LCST) = (5.38\%, 45.0°\text{C})$.
- forms dimers in water at all temperatures; this is implied by the value $r \approx 310$[2], and supported by the narrowing of spectral lines after the addition of acid, see the Figures 4.17, 4.18.
- will prefer to form complexes with cations instead of its own molecules if cations are available and this will cause the dimers to break down; supported by the same figures, the Figures 4.17, 4.18
- phase separation can be shifted to higher temperatures, or even prevented by the addition of *S*-CSA into the solution, compare the Figures 4.20–4.22; the constituent phases also become less well defined, compare the shapes of the C' peaks in the Figures 4.20 and 4.21. This is due to the hydrophilicity of *S*-CSA that excludes it from the β phase and its Coulombic attraction with the H^+ ions. *S*-CSA effectively increases the solubility of **3,4,5-TEG-TPP**
- in $CDCl_3$ no **3,4,5-TEG-TPP** phase separation was observed

These conclusions are supported by the OM results:

- upon heating, there are exactly two phases present after phase separation in an originally homogeneous and transparent sample.
- after some time the bulk of the porphyrin-rich β-phase droplets is low in H^+ content and the originally *green* acidic solution becomes *brownish* and *turbid*.
- over time, the β-phase droplets become larger (Ostwald ripening).

[2]The molar mass ratio of porphyrin to the molar mass of D_2O is approximately 128. $2560/20 = 128$.

5. Instrumentation and software

Laboratory instruments

All of the high-resolution NMR experiments were performed using the commercially available NMR spectrometers:

- Bruker Avance 500 MHz
- Bruker Avance III HD 500 MHz

The magnitudes of the magnetic fields of both are $B_0 = 11.7$ T, with equivalent ^{1}H Larmor frequency 500 MHz.

We used the TBO, TBI, BBO, BBFO probe types designated for liquid phase measurements.

During each scan we maintained constant sample temperature within ± 0.5 K range of the set values using the BVT 3000 and BCU 2 temperature control units, also commercially available from Bruker.

Software

As for the software used in creation of this thesis:

- TopSpin developed by Bruker [28] – NMR data acquisition and processing software that we also used to export all of the spectra and stack plots
- Jan Labuta's pre-made Excel files – for fitting most of the 1D NMR spectra
- Dmfit by Dominique Massiot et al. [29] – for fitting the most difficult spectra
- my own data-processing Python "notebooks" and scripts prepared using the Anaconda Python distribution by Continuum Analytics [26] – calculating everything other than the spectrum fits: f_{sep} fitting, binodal and spinodal fitting, all the plotting
- Inkscape, a free and open-source vector graphics editor [30] – all of the figure editing past plotting and spectra exports
- MiKTeX, the LaTeXdocument typesetting system for MS Windows operating systems – document creation
- Notepad++, a free text editor [31]– LaTeXsource code typing

Bibliography

[1] J. Chou *et al.*, *The Porphyrin Handbook: Applications of Porphyrins and Metalloporphyrins to Materials Chemistry*, vol. 6. Cambridge, Massachusetts: Academic Press, 2000.

[2] J. Labuta, S. Ishihara, A. Shundo, S. Arai, S. Takeoka, K. Ariga, and J. P. Hill, "Chirality sensing by nonchiral porphines," *Chemistry – A European Journal*, vol. 17, pp. 3558–3561, 2011.

[3] J. Labuta *et al.*, "Dynamic processes in prochiral solvating agents (pro-csas) studied by nmr spectroscopy," *Symmetry*, vol. 6, pp. 345–367, 2014.

[4] A. Shundo *et al.*, "Nuclear magnetic resonance signaling of molecular chiral information using an achiral reagent," *Journal of American Chemicl Society*, vol. 131, pp. 9494–9495, 2009.

[5] W. Caughey *et al.*, "Heme a of cytochrome c oxicase. structure and properties: comparisons with hemes b, c, and s and derivatives," *Journal of Biological Chemistry*, vol. 250, no. 19, pp. 7602–7622, 1975.

[6] J. Carter, "Photosynthesis," January 2015. University of Cincinnati, `http://biology.clc.uc.edu/courses/bio104/photosyn.htm`.

[7] K. Yamada, "Interrelations between essential metal ions and human diseases," *Metal Ions in Life Sciences*, vol. 13, no. 3, pp. 295–320, 2013.

[8] G. Färber *et al.*, "Coenzyme f430 from methanogenic bacteria : Complete assignment of configuration based on an x-ray analysis of 12,13-diepi-f430 pentamethyl ester and on nmr spectroscopy," *Helvetica Chimica Acta*, vol. 4, pp. 697–716, 1991.

[9] C. Leznoff, *Phthalocyanines, Properties and Applications*, vol. 1–4. John Wiley and Sons, 86.

[10] P. Raven *et al.*, *Biology of Plants*. London, England: W.H. Freeman and Company, 7 ed., 2005.

[11] H. Schneider, "Binding mechanisms in supramolecular complexes," *Angewandte Chemie International Edition*, vol. 48, no. Issue 22, pp. 3924–3977, 2009.

[12] H. Schneider *et al.*, "Dispersive interactions in supramolecular porphyrin complexes," *Tetrahedron*, vol. 58, pp. pp. 779–786, 2002.

[13] C. Martinez and I. BL, "Rethinking the term "pi-stacking".," *Chemical Science*, vol. 3, pp. 2191–2201, 2012.

[14] H. Schneider, "Dispersive interactions in solution complexes," *Accounts of Chemical Research*, vol. 48, no. Issue 7, pp. 1815–1822, 2015.

[15] G. Mamardashvili, "Tsolubility of alkylporphyrins," *Molecules*, vol. 5, pp. 762–766, 2000.

[16] M. Ward *et al.*, "Thermoresponsive polymers for biomedical applications," *Polymers*, vol. 3, pp. 1215–1242, 2011.

[17] PubChem, "L-Menthol," May 2016. `https://pubchem.ncbi.nlm.nih.gov/compound/_-_-menthol#section=Top`.

[18] PubChem, "Bupivacaine," May 2016. `https://pubchem.ncbi.nlm.nih.gov/compound/bupivacaine#section=Top`.

[19] Patrick Le Guennec, "Describing Chirality," May 2016. `http://www.chirality.org/homepage.htm`.

[20] K. Curry *et al.*, "Determination of monosodium glutamate enantiomers by chiral phase capillary gas chromatography," *Journal of High Resolution Chromatography :510-511*, vol. 6(9), pp. 510–511, 1983.

[21] M. Levitt, *Spin Dynamics: Basics of Nuclear Magnetic Resonance*. Reading, Massachusetts: John Wiley and Sons, 2 ed., 2008.

[22] H. Günther, *NMR Spectroscopy: Basic Principles, Concepts, and Applications in Chemistry*. Weinheim, Germany: John Wiley and Sons, 3 ed., 2013.

[23] P. Flory, *Principles of Polymer Chemistry*. New York City, NY: Cornell University Press, 1953.

[24] T. Tanaka, "Collapse of gels and the critical endpoint," *Physical Review*, vol. 40, pp. 820–823, 1978.

[25] V. O. Aseyev *et al.*, "Temperature dependence of the colloidal stability of neutral amphiphilic polymers in water," *Advances in Polymer Science*, vol. 196, pp. 1–85, 2006.

[26] Continuum Analytics, "Anaconda Python distribution," June 2015. `https://www.continuum.io/downloads`.

[27] Sigma Aldrich, "*S*-camphorsulfonic acid," May 2016. `http://www.sigmaaldrich.com/catalog/product/aldrich/c2107?lang=en`.

[28] Bruker, "TopSpin," May 2016. `https://www.bruker.com/products/mr/nmr/nmr-software/software/topspin/overview.html`.

[29] D. Massiot *et al.*, "Modelling one- and two-dimensional solid-state nmr spectra," *Magnetic Resonance in Chemistry*, vol. 40, pp. 70–76, 2002.

[30] Tavmjong Bah, "Inkscape Project Website," May 2016. `https://inkscape.org/en/`.

[31] Don Ho, "Notepad++," May 2016. `https://notepad-plus-plus.org/`.